ELSEVIER

Contents lists available at ScienceDirect

Remote Sensing of Environment

journal homepage: www.elsevier.com/locate/rse





Mapping smallholder cashew plantations to inform sustainable tree crop expansion in Benin

Leikun Yin ^a, Rahul Ghosh ^b, Chenxi Lin ^a, David Hale ^c, Christoph Weigl ^{c,d}, James Obarowski ^e, Junxiong Zhou ^a, Jessica Till ^a, Xiaowei Jia ^f, Nanshan You ^a, Troy Mao ^g, Vipin Kumar ^b, Zhenong Jin ^{a,*}

- ^a Department of Bioproducts and Biosystems Engineering, University of Minnesota, St. Paul, MN 55108, USA
- ^b Department of Computer Science and Engineering, University of Minnesota, Minneapolis, MN 55414, USA
- ^c TechnoServe Labs, Arlington, VA 22209, USA
- d McKinsey & Company, New York City, NY 10022, USA
- e PULA, Nairobi, Nairobi County 00100, Kenya
- f Department of Computer Science, University of Pittsburgh, Pittsburgh, PA 15260, USA
- g College of Letters and Science, University of California, Davis, CA 95616, USA

ARTICLE INFO

Edited by Dr. Marie Weiss

Keywords:
Tree crop mapping
Smallholder agriculture
Deep learning
Cashew plantation
Planet Basemaps

ABSTRACT

Cashews are grown by over 3 million smallholder farmers in >40 countries worldwide as a principal source of income. Expanding the area of cashew plantations and increasing productivity are critical to improving the livelihood of many smallholder communities. As the third largest cashew producer in Africa, Benin has nearly 200,000 smallholder cashew growers contributing 15% of the country's national export earnings. Expansion of the cashew industry is thus an essential economic driver and a governmental priority in Benin. However, a lack of information on where and how cashew trees grow across the country hinders decision-making that could support increased cashew production and poverty alleviation. By leveraging 2.4-m Planet Basemaps and 0.5-m aerial imagery, two newly developed deep learning algorithms, and large-scale ground truth datasets, we successfully produced the first-of-its-kind national map of cashew in Benin and characterized the expansion of cashew plantations between 2015 and 2021. In particular, we developed a SpatioTemporal Classification with Attention (STCA) model to map the distribution of cashew plantations with 2.4-m multi-temporal Planet Basemaps from 2019 to 2021, which can fully capture texture information from discriminative time steps during a growing season. The U-Net model was employed to map the distribution of cashew plantation with 0.5-m mono-temporal aerial imagery in 2015, which can achieve accurate and fast predictions even with limited training data. We further developed a Clustering Augmented Self-supervised Temporal Classification (CASTC) model to distinguish high-density versus low-density cashew plantations by automatic feature extraction and optimized clustering. Results show that the STCA model has an overall accuracy over 85% based on 1400 ground truth point samples from each year. The CASTC model achieved an overall accuracy of 76% based on 348 ground truth samples of planting density. We found that the cashew area in Benin has almost doubled to 519 \pm 20 kha from 2015 to 2021 with 60% of new plantation development coming from cropland or fallow land, while encroachment of cashew plantations into protected areas has increased by 55%. Only about half of cashew plantations were high-density in 2021, suggesting high potential for intensification. Our study illustrates the power of combining highresolution remote sensing imagery and state-of-the-art deep learning algorithms to better understand tree crops in the heterogeneous smallholder landscape, which can help efficiently allocate limited training and nursery resources for sustainable agricultural development.

E-mail address: jinzn@umn.edu (Z. Jin).

^{*} Corresponding author.

1. Introduction

Achieving zero hunger and ending poverty by 2030 are two primary and vital missions of the United Nations (UN) Sustainable Development Goals (UN, 2015). Poverty is a leading cause of hunger, which continues to affect many people in food-insecure regions of South Asia and Sub-Saharan Africa (Lowder et al., 2016; Samberg et al., 2016). Most research and applications in the field of food security focus on increasing staple crop production in the developing world, e.g., through crop yield forecasts (Basso and Liu, 2019) and early warning of famine situations (Becker-Reshef et al., 2020). However, these areas of scientific exploration cannot resolve the underlying problem of poverty for countries in the Global South. For smallholder farmers, growing tree crops can provide a stable source of income because of their relatively high cash value, predictable yields, long tree lifespans of 20-30 years, and good adaptability to growth conditions (Lin et al., 2021). With tens of millions of smallholder farmers in tree crop production (cashew, cocoa, coffee, etc.), tree crops contribute a large percentage of income in poor communities globally (Waarts et al., 2021). Increasing the production of tree crops is therefore an important and effective way to improve the living conditions of smallholders.

Cashew tree crops are widely farmed in 46 countries across Africa, Asia, Latin America, and the Caribbean, 18 of which are among the least developed countries. Africa accounts for more than half of global raw cashew nut production, followed by Asia, and ~ 80% of Africa's raw cashew nut production is concentrated in West Africa, principally in Côte d'Ivoire, Nigeria, Benin, and Guinea-Bissau. However, <10% of the world's raw cashew nuts are processed in Africa, with the majority (>85%) processed in Asia, primarily in Vietnam and India (UNCTAD, 2021). In addition to cashew nuts, the by-products of the cashew crop have a variety of industrial uses that can help smallholders diversify their sources of income. Cashew nut shell liquid has the potential to be used as a biofuel (Sanjeeva et al., 2014), and cashew apples can be used to produce a range of beverages and animal feed (Gomes et al., 2018). Since cashew tree crops are typically cultivated by smallholder farmers, value additions in the cashew industry and poverty reduction are tightly connected.

Benin is among the top ten cashew growers in the world and the third largest cashew nut producer in West Africa (Duguma et al., 2021). Cashew nuts from Benin are renowned for their superior quality and bright white hue. The government of Benin recognizes the importance of cashew tree plantations in the fight against poverty for smallholder farmers, as evidenced by their strategy to double cashew production from 2016 to 2021 in the government action plan - Benin Revealed: Government Action Program (MAEP-Benin, 2017) - and the subsequent 2022-2026 plan (PNIASAN-Benin, 2022). There are two main ways to increase cashew nut production. The first strategy is to expand the area under cultivation by converting other land use types. The second is to improve the use of good agricultural practices (GAP) on existing cashew plantations to increase yield. Both strategies require detailed knowledge of the location of cashew growing areas around the country and GAP implementation, including planting density (tree spacing). Periodic mapping to obtain data on the spatial distribution and density of cashew plantations can therefore help governments understand and adjust policies regarding land use conversion and to efficiently manage field extension services. In addition, identifying regions where cashews have been planted with suboptimal planting density according to GAP guidelines can help direct needed resources, including the provisioning of new cashew nurseries that are a core part of Benin's national cashew strategy and are crucial to increasing production. In Benin and many other countries in sub-Saharan Africa, the traditional method of gathering information about cashew plantation distribution and GAP related to tree density is through extensive field data collection by conducting in-person farm visits and field surveys, which are inefficient and laborious on a large scale. Efficient and low-cost measures are urgently needed to assist the implementation of development programs on a

national scale (Burke and Lobell, 2017; Chivasa et al., 2017).

Remote sensing offers a cost-effective and time-saving way to characterize ground objects and track surface changes over time at a large scale. Agricultural remote sensing has made significant contributions to fighting food insecurity through mapping crop types, predicting yields, and monitoring crop diseases/insect pests and more (Atzberger, 2013; Maes and Steppe, 2019; Nellis et al., 2009; Sishodia et al., 2020). However, research involving remote sensing and tree crops is mostly concerned with mapping tree crops and the effects of deforestation, with an emphasis on oil palm (Cheng et al., 2016; Gutiérrez-Vélez and DeFries, 2013; Xu et al., 2022) and rubber (Dong et al., 2013; Tridawati et al., 2020) trees. Rubber and oil palm trees have relatively prominent spatial and spectral features and are often grown in commercial farmlands spanning a few kilometers (Putra and Wijayanto, 2023; Lin et al., 2021). This reduces the need for high spatial resolution imagery, so that even 250-m MODIS images can be used to map them (Jia et al., 2016; Jia et al., 2020). In contrast, certain essential global commodity tree crops have smaller crowns (< 5 m) and are planted in small plots (under 5 ha or 50,000 m²) with irregular patterns (Lin et al., 2021; Meyfroidt et al., 2013). Regarding cashew trees, although their crown diameters can reach 6–15 m (Preedy and Watson, 2020), newly established plantations in Benin frequently exhibit even smaller crown sizes (< 5 m), complicating classification through medium-resolution imagery. This is attributable to the cashew industry's rapid development in Benin due to its superior economic benefits compared to staple crops, leading to the swift establishment and expansion of new cashew plantations with seedlings. Furthermore, based on 3998 field-surveyed cashew plantation borders, we discovered that over 70% of cashew plantations in Benin occupy an area of 2 ha or less, and nearly 95% have an area of 5 ha or less (Table S1). In Benin, the fragmented nature of cashew plantations and their small canopies render high-resolution imagery a more suitable data source. In general, cashew plantations have received significantly less attention in the past than other tree crops, with the exception of some local-scale studies in a specific community or national park with medium resolution (10-30 m) remote sensing imagery and simple machine learning methods such as Random Forest, Support Vector Machines, and Classification and Regression Trees (Pereira et al., 2022; Rege et al., 2022; Singh et al., 2018). Those approaches are not transferable to national-scale studies and are insufficient to resolve individual fields that are particularly relevant to smallholder management practices. This is because simple machine learning methods have difficulty in extracting local features or learning spatial hierarchies of feature patterns (Alzubaidi et al., 2021; Boston et al., 2022; LeCun and Bengio, 1995; Yamashita et al., 2018; Zhang et al., 2022). Such methods were also not originally designed to process multi-temporal data (Xu et al., 2020), which impairs their transferability. Furthermore, in tropical regions, mapping smallholder tree crops remains challenging given the fragmentary landscape and lack of cloud-free observations by many satellite sensors. Although efforts have targeted smallholder plantation systems and complex landscapes (Ballester-Berman and Rastoll-Gimenez, 2021; Descals et al., 2019; Dong et al., 2012; Maskell et al., 2021), these studies utilized medium-resolution spatiotemporal satellite imagery (e.g., Landsat and Sentinel-2) that possesses limited spatial resolution and insufficient cloud-free observations for small-crown tree crops (< 5 m). Even fewer studies address different intra-class management practices, e.g., coffee sub-categories (Hunt et al., 2020; Kawakubo and Pérez Machado, 2016; Maskell et al., 2021). In recent years, in addition to aerial and drone imagery, as a number of microsatellite constellations have been launched by private aerospace companies such as Planet, Airbus, and DigitalGlobe, more data sources are available for high-resolution mapping (< 3 m). However, only limited small-scale case studies of ~ 1000 km² or less have leveraged highresolution data to map smallholder tree crops (Burnett et al., 2019; Cui et al., 2022).

To understand smallholder cashew plantations in Benin and fill the gap in large-scale small-crown tree crop mapping with high-resolution imagery, we employed Planet Basemaps (2.4 m) and aerial imagery (0.5 m) with advanced spatiotemporal deep learning techniques to map cashew plantation distribution and planting density in Benin. Several aspects of smallholder cashew plantations made the two classification tasks challenging. First, cashew trees of different varieties and ages grow in the same plantation with irregular spacing, which results in tremendous intra-plantation heterogeneity. Second, there is often large interplantation heterogeneity in terms of size, shape, and planting density. In this case, sensors with medium spatial resolution (e.g., Sentinel-2 and Landsat) and simple machine learning classification algorithms have difficulty mapping smallholder cashew plantations at the field level (Ghimire et al., 2010; Peña-Barragán et al., 2011; Rao et al., 2021; Rufin et al., 2022). Finer remote sensing products (such as the 2.4-m Planet Basemaps and 0.5-m aerial imagery used here) and advanced deep learning techniques have opened up new possibilities for monitoring smallholder cashew plantations. Additionally, the spectral signal distortion from omnipresent clouds and shadows can be overcome by the daily revisit frequency of Planet imagery, which can provide cloudfree Planet Basemaps on a monthly basis. Our study employed multitemporal Planet Basemaps and the proposed SpatioTemporal Classification with Attention (STCA) model to map cashew plantations from 2019 to 2021. Because wall-to-wall Planet Basemaps were not available before 2019, mono-temporal aerial imagery and a U-Net model were also used to map cashew plantations in 2015. Additionally, we distinguished two kinds of cashew planting density using the proposed Clustering Augmented Self-supervised Temporal Classification (CASTC) model for 2021.

To our knowledge, this is the first-of-its-kind large-scale cashew plantation map leveraging high-resolution remote sensing imagery. In this study, we (i) developed spatiotemporal tree classification algorithms for cashew, (ii) mapped cashew plantation spatial distributions for four years (2015, 2019, 2020, and 2021), (iii) tracked the spatiotemporal changes in cashew plantations, and (iv) distinguished high-and low-density cashew plantation management practices. While this study focuses on cashew tree crops in Benin as a special case, the derived

classification algorithm can help inform cashew mapping in other countries or be used for other similar tree crops.

2. Data and methods

2.1. Study area

The Republic of Benin comprises 12 departments (the primary administrative units) and is subdivided into 77 communes. The study area located in central Benin (1–3°E, 7–10°N) is one of the primary cashew-growing regions in West Africa, which spans 12 communes in four departments - Donga, Borgou, Collines, and Zou. (Fig. 1(a)). Heterogeneous landscapes are prevalent here (Fig. 1(b)), and cashew trees are typically cultivated in smallholder plantations of <5 ha.

The study region has a tropical savanna climate, and its typical yearly temperature ranges from 24 to 31 °C. In the study region, the dry season lasts from November to April, while the rest of the year makes up the rainy season (Table 1). Drought conditions are concentrated between December and January during the dry season, while the wettest months occur from June to September during the rainy season. The planting time for cashew tree seedlings is during the rainy season, mainly between July and August. The cashew tree blossoms and produces fruit mainly during the dry season. The peak flowering period for the cashew tree lasts from December through January and cashew nut harvest typically takes place from February through March.

2.2. Imagery

2.2.1. Planet Basemaps

The Planet Basemaps are 4-band (blue, green, red, and near infrared, i.e., RGB + NIR) surface reflectance (SR) product composed of images captured by the PlanetScope microsatellite constellation (Fig. S1(b)-(c)), a collection of hundreds of microsatellites carrying three generations of sensors (Dove Classic, Dove-R, and SuperDove). The raw imagery has a resolution of about 3 m spatially and about 1 day temporally (Planet,

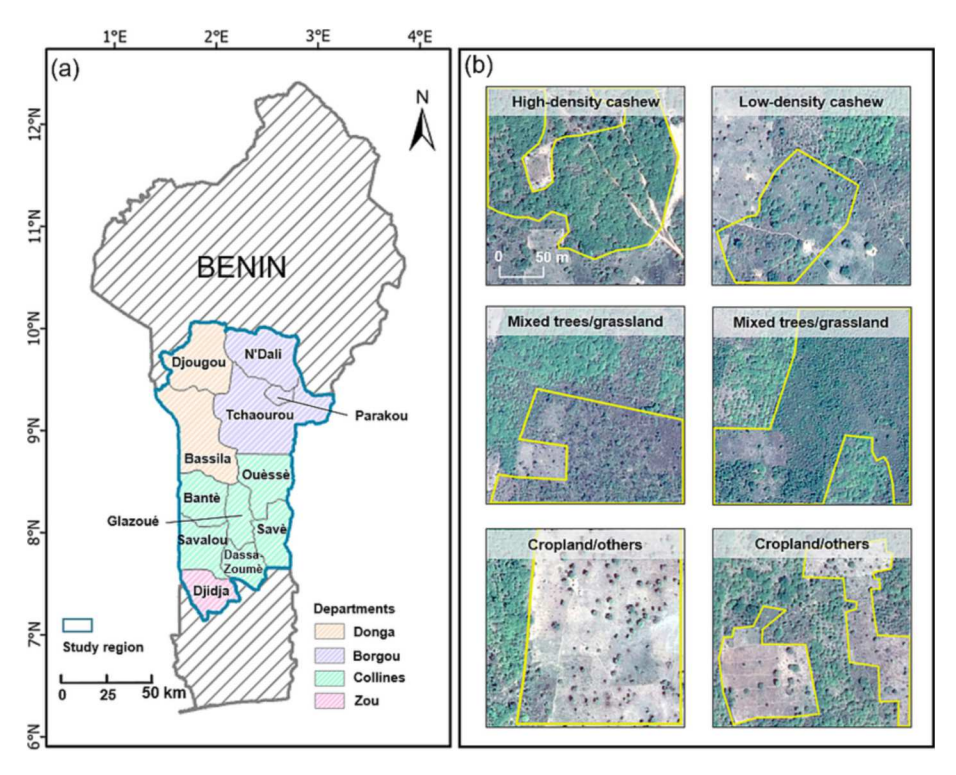


Fig. 1. (a) Location of the study region and administration map. (b) Sample cashew plantation, mixed trees/grassland, and cropland/others. The extents enclosed by the yellow boundaries correspond to the categories noted. (For interpretation of the references to colour in this figure legend, the reader is referred to the web version of this article.)

Table 1

Average precipitation in millimeters per month from 2015 to 2021 (CHIRPS) and cashew crop calendar in which dark colors indicate more concentrated events.

		May	June	July	Aug.	Sept.	Oct.	Nov.	Dec.	Jan.	Feb.	Mar.	Apr.
Precipitation (mm/month)	Rainy	134	164	198	205	203	114						
	Dry							11	4	3	11	59	75
Cashew crop calendar	Planting												
	Flowering												
	Harvest												

2022a). Between Dec. 1st, 2019 and Nov. 30th, 2020, the global mean probability of at least one cloud-free observation over a 5-day period was 0.84, while that of at least two observations was 0.65 (Roy et al., 2021). Compared to medium-resolution satellite imagery products, such as Landsat and Sentinel-2, Planet Basemaps offer superior spatial resolution and diminished cloud and shadow effects. The Planet Basemaps are organized in tiles, with 569 tiles required each month to fully cover the study region. Planet Basemaps are available in either Zoom Level 15 (4.77 m) or Zoom Level 16 (2.38 m); we opted for the latter, given its better observational capability. Between 2019 and 2021, the Planet Basemaps served as the source data for mapping cashew plantations. These Basemaps were obtained through Planet's Education and Research Program licensed to the University of Minnesota.

In the production of Planet Basemaps, an initial raw scene (a single image captured by a PlanetScope satellite) undergoes radiometric calibration and atmospheric corrections (Planet, 2022b). Subsequently, Planet Basemaps are constructed through two primary steps - scene selection and normalization. The optimal monthly scene for Basemap construction is determined based on various image quality metrics (e.g., cloud cover and image sharpness), with the highest-ranking imagery utilized in subsequent normalization (Planet, 2019). To enhance spatial and temporal consistency of data from disparate sensors, normalized Basemaps are developed by fitting a scene-specific normalization model (a constrained linear model) based on the co-located PlanetScope SR and Sentinel-2-based seasonal reference pixels (Kington et al., 2019). The normalization model is established for each scene to guarantee spatial consistency within a scene and to correct various sources of variability between sensors and scenes within the PlanetScope constellations (e.g., BRDF effects). The seasonal reference dataset constitutes a static, multiyear seasonal imagery, rather than near-coincident Sentinel-2 imagery, ensuring a reference dataset free of cloud, haze, and snow, even in exceptionally cloudy tropical regions (Planet, 2022c). The objective function of the scene-specific normalization model encompasses two components: the misfit metric, which quantifies how well the model fits the pixels from the PlanetScope scene and the seasonal reference dataset, and the regularization metric, which penalizes solutions where one band would change drastically more than others during normalization. Ultimately, after images are mosaicked into image tiles, a seamlinereduction algorithm is applied to minimize local differences between images (Planet, 2019).

Although the normalization preprocessing of Planet Basemaps often improves consistency with Sentinel-2 images, it also introduces potential issues (Planet, 2022c). First, the significant differences in spectral response between Dove sensors necessitate varied degrees of correction during normalization. Specifically, Dove Classic requires more substantial corrections, leading to systematic discrepancies in its normalized products due to its significant divergence from Sentinel-2. Second, regionally-extensive rapid and unexpected changes like unanticipated droughts or extensive harvesting can disrupt the normalization process, leading to overcorrections. While Planet's normalization model generally manages phenomena like deforestation, snow, clouds effectively,

sudden regionally extensive changes could cause issues.

2.2.2. Aerial imagery

Aerial imagery was employed for cashew plantation mapping in 2015 due to the fact that Planet Basemaps are not available prior to 2019. The aerial imagery came from a project supervised by the Benin government for the preservation and development of gallery forests and digital base mapping production. A fixed wing aircraft, a Piper PA-31 Navajo, was used for imagery collection in May 2015. A multispectral camera (UltraCam Eagle Mark 3) with a focal length of 40 mm was mounted on the airplane platform to collect ground information in four spectral bands (RGB + NIR) from 3 km above the ground (Fig. S1(a)-(b)). Radiometric correction, geometric correction, and orthorectification have been applied to develop a SR product that is organized in grids. The cloud-free SR product has a spatial resolution of 0.5 m, and 2031 tiles were required to fully cover the study region.

2.2.3. Imagery for the training region

In addition to Planet Basemaps and aerial imagery encompassing the entire study area, we employed three further types of source data within the training region: an Airbus Pleiades Pan-sharpened Standard Ortho product, a Sentinel-2 Level-2A (L2A) product, and Planet Daily Scenes. The Airbus Pleiades product served as a labeling reference in 2020, while Sentinel-2 L2A and Planet Daily Scenes were utilized in an experiment comparing classification outcomes from three distinct source data types - Planet Basemaps, Sentinel-2 L2A, and Planet Daily

The Pleiades constellation is composed of two satellites (Pleiades-1A and -1B) that supply 0.5-m panchromatic and 2-m multispectral (RGB + NIR) images (Pleiades, 2012). The product employed in this study is an orthorectified SR product featuring four 0.5-m bands, which were converted from four 2-m multispectral bands through fusion with a 0.5-m co-registered panchromatic image. The imagery was captured in March 2020 and obtained from our collaborator, TechnoServe.

The MSI sensor equipped on Sentinel-2 features 13 bands and is frequently employed for crop classification. The Sentinel-2 L2A SR product has undergone radiometric calibration, atmospheric correction, and geometric correction (ESA Sentinel-2 User Handbook, 2015; Gascon et al., 2017; Yan et al., 2018). Ten bands (RGB + NIR of 10 m along with red-edge and SWIR bands of 20 m) were selected to evaluate the classification performance against Planet data. For consistent spatial resolution among bands, we upscaled six 20-m bands to 10 m using nearest neighbor method. To mask out cloudy observations, a cloud score algorithm developed for Landsat images (Oreopoulos et al., 2011) was adapted to Sentinel-2. Specifically, five bands (RGB, Aerosol and Cirrus bands) along with two spectral indices (normalized difference moisture index (Gao, 1996) and normalized difference snow index (Hall et al., 1995)) were employed to calculate cloud score and identify clouds, considering that clouds are reasonably bright in cirrus and visible bands and are moist. The modified cloud score algorithm demonstrated superior cloud detection accuracy compared to the QA60 quality assessment

band (You and Dong, 2020). Given there is no cirrus band in Sentinel-2 L2A, we employed bands from Sentinel-2 L1C to generate a cloud mask and apply it to Sentinel-2 L2A. To generate monthly composites, we selected the median value of all available data for each pixel for each month between November and May (Teluguntla et al., 2018; You and Dong, 2020) of 2020. The Sentinel-2 L2A data was downloaded and preprocessed on Google Earth Engine (Gorelick et al., 2017).

Planet Daily Scenes originate from images captured by the Planet constellation and represent an SR product that has undergone radiometric calibration and atmospheric corrections (Planet, 2022b). They comprise four bands (RGB + NIR) with a spatial resolution of 3 m. To reduce the cloud of Planet Daily Scene, we set the parameter "cloud cover" to be $<\!10\%$ on Planet Explorer and downloaded the filtered data. The monthly composites were generated in the same way as for Sentinel-2 L2A. This data was procured through the Planet's Education and Research Program licensed to the University of Minnesota.

2.3. Ground truth survey

2.3.1. Training data

Our chosen region for training the classification algorithms is an area of 1000 km² (Fig. 2), containing heterogeneous landscapes and irregular smallholder cashew plantations that are appropriate for training and selecting the optimal deep learning model. A ground survey conducted through the TechnoServe BeninCajù program collected detailed land cover types and aggregated them into four categories: cashew plantations, mixed trees/grassland, built-up land, and cropland/others. Based on this survey map, we manually delineated ground truth polygons for these four categories using 0.5-m aerial imagery in 2015 and Airbus imagery in 2020 to map cashew plantation distributions in 2015 and from 2019 to 2021, respectively. The training region in Fig. 2 shows labeled examples from Airbus imagery. The mixed trees/grassland class includes mixed scattered trees, grassland, and gallery forest, while the cropland/others class mainly includes cropland and bare land. A resampling was applied to address the mismatch between the training labels based on 0.5-m imagery when they are directly applied to the 2.4m Planet Basemaps. Because resampling from the manual ground truth to the Planet-based ground truth would cause a mixture of boundary pixels between two land cover types, we performed a 2-pixel erosion for each class, then relabeled eroded pixels as the cropland/others class and

removed connected pixel clusters of <30 pixels.

For mapping cashew planting density, we defined high-density and low-density cashew plantations as having > or <100 trees/ha, respectively. In production practice, optimal yield is achieved in high-density plantations with a planting density between 100 and 180 cashew trees/ha. Low-density planting (< 100 trees/ha) cannot fully exploit the productive potential of cropland, while a density of over 180 trees/ha can lead to declining productivity due to quality issues caused by disease and infestation. Although here we used a threshold of 100 trees/ha to distinguish between low-density and high-density cashew plantations, future studies will use a more in-depth classification that includes "veryhigh-density" plantations above 180 trees/ha.

2.3.2. Sampling strategy and validation

Our sampling strategy follows a probability sampling protocol (Olofsson et al., 2014) and consists of two phases to generate unbiased area estimates with uncertainties. In the first phase, we performed a simple random sampling method at the cluster level. The study region was divided into 5 by 5 km clusters totaling 1663 clusters (Fig. 2), where the 5-km cluster size ensured the inclusion of a large number of smallholder fields. Of these, we discarded 241 clusters that were located on the study area boundary. The remaining 1422 clusters were retained for probability sampling, from which 120 sample clusters were randomly selected. In the second phase, we implemented a stratified random sampling method at the pixel level in the selected clusters. This sampling strategy significantly reduces the workload of visual interpretation by constraining sample pixels into these clusters. Specifically, according to our three mapped classes (mixed trees/grassland, cashew plantations, and cropland/others) we first generated four land-use change classes between successive years to estimate the area of source classes that account for cashew plantation expansion. Then, we constructed seven strata consisting of the three stable land cover classes and the four land cover change classes (listed below). We allocated the sample size in proportion to strata area, but slightly increased the sample size for less frequent classes, i.e., land-use change classes. This approach helps to balance the trade-off between user's, producer's, and overall accuracies (Olofsson et al., 2014). The seven strata of stable mixed trees/grassland, stable cashew plantations, stable cropland/others, change from mixed trees/grassland to cashew, change from cropland/others to cashew, change from mixed trees/grassland to cropland/others, and change from

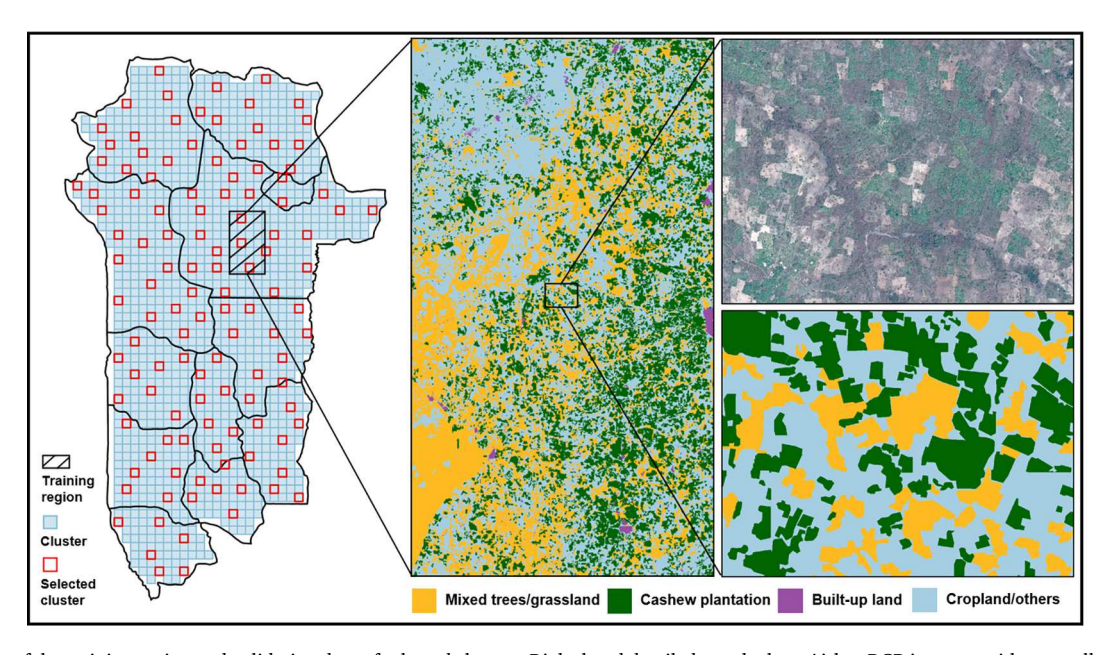


Fig. 2. Locations of the training region and validation data of selected clusters. Right-hand detailed panels show Airbus RGB imagery with manually delineated labels for comparison.

cropland/others to mixed trees/grassland contain 300, 200, 400, 100, 100, 100, 100, and 200 sample points, respectively. A total of 1400 sample pixels were selected for visual interpretation for each year. Five types of auxiliary information were additionally displayed to help visually interpret sample pixels: (1) 2.4-m temporal Planet Basemaps from 2019 to 2021, (2) 0.5-m aerial imagery for 2015, (3) high-resolution imagery from Google Earth Pro, (4) 11,397 field-collected cashew plantation boundaries, and (5) >1100 field-collected and visually interpreted samples labeled by TechnoServe. The reason why we didn't use the field samples directly was that they were collected before this study and did not consider the need for unbiased accuracy and area estimation. In accordance with prior studies (Olofsson et al., 2013; Olofsson et al., 2014; Stehman, 2014), we adjusted the accuracy and area estimation by considering the area of each stratum and generated 95% confidence intervals.

Furthermore, as the cashew tree is a perennial plant, we used 196 cashew plantation ground truth samples with the same exact location across the four years to validate the consistency of our classification maps in each of the four years. We also used 348 field-collected samples

with known planting densities to assess the accuracy of cashew plantation planting density determinations. Prior to the ground survey, we selected validation point locations that allowed for both transportation accessibility and widespread distribution of the samples. Enumerators then used GPS devices to locate the predetermined samples and noted the planting density.

2.4. Methodology

2.4.1. Tree crop mapping algorithms for cashew plantations

This study proposes tree crop mapping algorithms for cashew plantations that address both the spatial distribution and planting density in two stages (Fig. 3). At the distribution mapping stage, the SpatioTemporal Classification with Attention (STCA) model was developed and U-Net (Ronneberger et al., 2015) was applied to map cashew plantation distributions for multi-temporal imagery from 2019 to 2021 and for mono-temporal imagery in 2015, respectively. At the planting density mapping stage, the Clustering Augmented Self-supervised Temporal Classification (CASTC) model was developed to map cashew planting

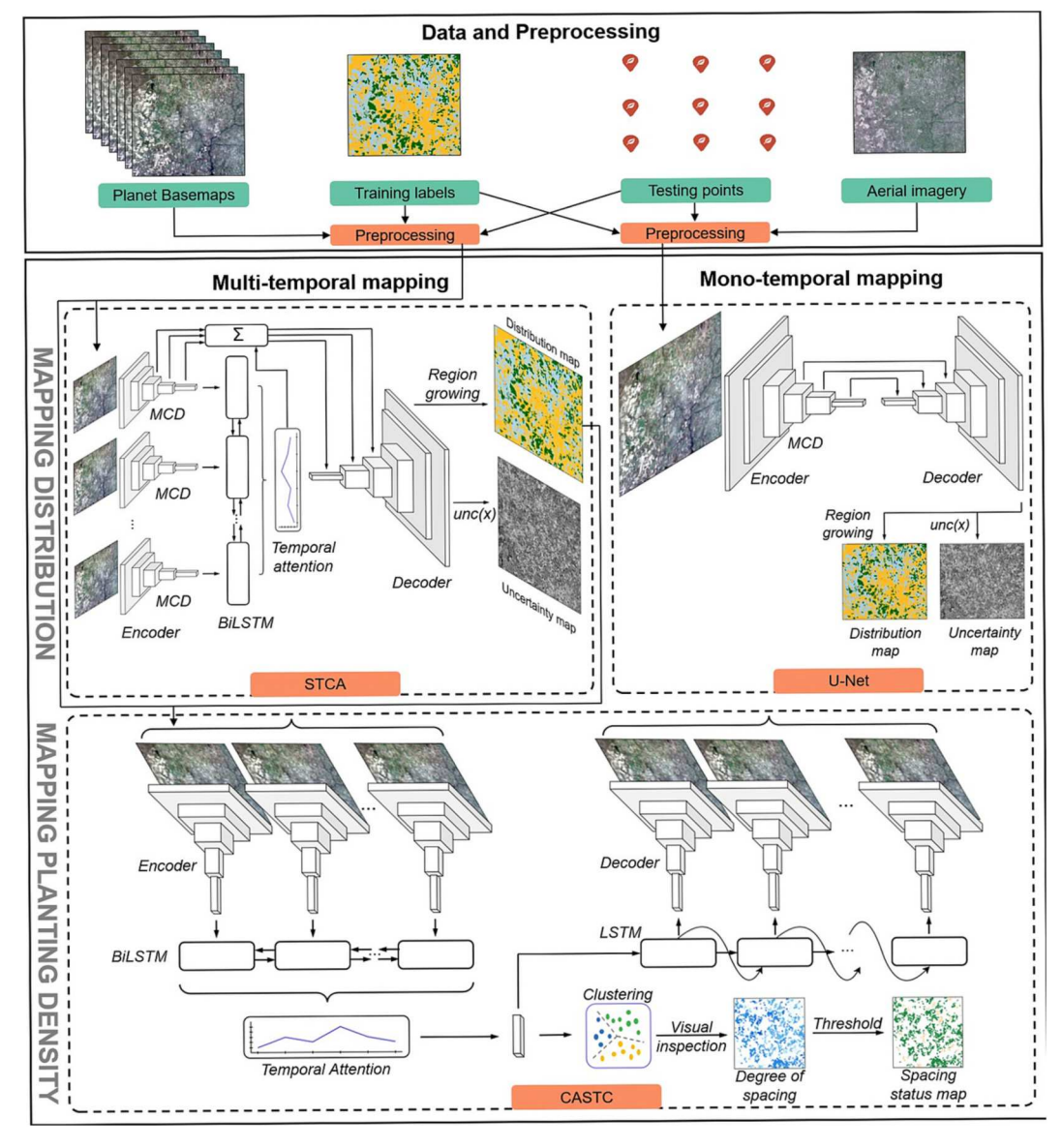


Fig. 3. Overview of tree crop mapping algorithms for cashew plantations along with the data and methods employed, and the maps generated. There are two branches for multi-temporal and mono-temporal imagery, respectively. Each deep learning module is enclosed by a dotted box. MCD indicates Monte Carlo dropout, and unc(x) is defined by Eq. (4).

density for multi-temporal imagery in 2021.

The training and testing steps using multi-temporal Planet Basemaps were conducted in a NVIDIA V100 GPU with 32 GB memory. Training and testing using mono-temporal aerial imagery were conducted in two NVIDIA V100 GPUs with 64 GB memory. For both sets of imagery, we used the same PyTorch deep learning framework.

2.4.2. Mapping the distribution of cashew plantations

2.4.2.1. Smoothing SR differences between tiles. Each Planet Basemap is a composite image made up of images from different microsatellites in the PlanetScope constellation, and therefore sometimes has issues with inconsistent SR for the same ground object between tiles, even after the correction by the Sentinel-2-based seasonal model (Houborg and McCabe, 2018; Rao et al., 2021). In addition, various levels of clouds and shadows also lead to multiform SR for the same ground object in different regions, despite the superior image quality of Planet Basemaps relative to the SR products of Sentinel-2 and Landsat imagery in the tropics. Some studies have partly addressed this problem by using the relatively mature SR products from Sentinel-2 and Landsat to stretch the histograms of Planet imagery (Jain et al., 2016; Rao et al., 2021). However, this method is unsuitable for our study region because Sentinel-2 and Landsat data have much more cloud coverage than Planet Basemaps in the tropics. Given that a small area has a high chance of being captured by the same sensor under similar cloud and shadow conditions, we split our study region into many small areas. To smooth SR differences between tiles, we then performed a normalization on each of them using Eq. (1), where $P_{normalized}$ is the normalized pixel value, P is the original pixel value, and P_{min} and P_{max} are the minimum and maximum pixel values respectively. In this study, we split our study region into 469 small regions according to the Planet Basemap tile boundaries for convenience. Each small region consists of a center tile and multi neighboring tiles extended from it. Note that we removed pixel values in the top and bottom two percentiles to avoid abnormal values. The same preprocessing was applied to aerial imagery. One caveat to note here is that, with the preprocessing of smoothing SR differences between tiles, the actual SR signal has been altered, and our classification method can perform better with smoothed SR in cloudy regions. It is a particularly useful step for alleviating spectral variability for the same kind of ground object when transferring the trained classifier to the whole study region (See Supplementary Text 1 for details).

$$P_{normalized} = \frac{P - P_{min}}{P_{max} - P_{min}} \tag{1}$$

2.4.2.2. Cashew plantation maps. We employed the STCA model to create cashew plantation maps for years from 2019 to 2021 using the Planet Basemaps. The STCA model can leverage the spatiotemporal information from time-series imagery to create a high-confidence cashew plantation map. Although several deep learning approaches that leverage spatiotemporal information for crop mapping (Ji et al., 2018; Jia et al., 2017; Mazzia et al., 2019) have shown encouraging results in isolated scenarios for studying a specific crop, these approaches used Convolutional Neural Networks (CNN) and Recurrent Neural Networks (RNN) in a straightforward manner to model spatial and temporal information without determining how various time steps contribute to the classification performance. Instead, we need a model that can automatically pay attention to the time steps that contribute the most to classification performance. The STCA model uses a U-Net-like module to automatically extract spatial features and a Bidirectional Long-Short Term Memory (BiLSTM) module (Graves and Schmidhuber, 2005) to extract phenological changes (Ghosh et al., 2021). To better aggregate the information for each time step, we further added the attention mechanism to aggregate the hidden representations over the time series based on their contribution to the classification performance (Luong et al., 2015; Jia et al., 2019). The parameter set θ of STCA was trained to

minimize the objective function of pixel-wise cross entropy on the limited number of manually annotated labeled patches:

$$\mathcal{L}(\theta \mid X, Y) = -\frac{1}{N \times 64 \times 64} \sum_{i=1}^{N} \sum_{(h,w)}^{(64,64)} \sum_{k=1}^{4} (Y_i)_{h,w}^{k} logf(X_i; \theta)_{h,w}^{k}$$
 (2)

where, N is batch size, X_i and Y_i denote the i^{th} patch in the batch and its corresponding label of size (h, w), and $f(X_i; \theta)$ is the predicted probabilities of each class k on the i^{th} patch. In this study, we used the kernel of 3 by 3 pixels for five convolution layers and the kernel of 2 by 2 pixels for max-pooling and transposed convolution layers in encoder and decoder.

For each year, imagery data for the seven months from November to May were fed into STCA. Before model training, each image tile was cut into image patches of 64 by 64 pixels. To create a more stable prediction result and quantify prediction uncertainty, Monte Carlo dropout was used in the testing phase. For standard deep learning models, dropout is only applied during training, which serves as a regularization to avoid overfitting. In our study, dropout was also applied in the testing phase. Specifically, we randomly sampled the neurons to be dropped out in each hidden layer, resulting in a slightly different model architecture, which can be viewed as an averaged ensemble of multiple different neural networks (Gal and Ghahramani, 2016). During testing, the predicted probability value for each class was obtained by taking the average of ten runs, as demonstrated in Eq. (3):

$$f(X_i) = \frac{1}{10} \sum_{r=1}^{10} f(X_i; \theta_r)$$
 (3)

where X_i denotes the i^{th} patch and $f(X_i; \theta_r)$ is the predicted probability of each run r on the i^{th} patch. Moreover, the standard deviation across the runs gives an estimate of the uncertainty unc in the prediction (Eq. (4)). In this study, the dropout rate is 0.3.

$$unc(X_i) = \sqrt{\frac{\sum_{r=1}^{10} (f(X_i; \theta_r) - f(X_i))^2}{10}}$$
 (4)

Next, each pixel was allocated a category using a region growing strategy. Traditionally, for deep learning multi-classification tasks, each pixel is assigned to the class with the highest Softmax value, and we refer to this strategy as "Argmax" prediction. However, with Argmax prediction, misclassification between spectrally similar classes and fragmentation of fields can easily occur. In our study, cashew plantations share similar spectral features with gallery forests and other tree crops, e.g., for some pixels which should be gallery forests or other tree crops, the highest Softmax value may be for cashew plantations. In this case, the Argmax prediction would wrongly classify these pixels as cashew plantation. In addition, the space between cashew trees in plantations may be identified as other land cover types, resulting in unrealistically fragmented fields. Therefore, the region growing strategy was chosen to process the pixel-wise Softmax output instead of directly taking Argmax prediction as a classification result. Specifically, step 1 in Fig. 4(a) shows the original Softmax output for one class, where darker blue colors represent larger Softmax values. As shown in step 2, pixels having a Softmax value >0.8 were assigned as seed pixels, and those between 0.4 and 0.8 were assigned as neighboring pixels. In step 3, neighboring pixels with a seed pixel in their neighborhood were reassigned as seed pixels. Step 4 shows the region growing result generated by seed pixels. The neighboring pixels in case 1 would not be maintained in the end, which reduces misclassification, while the neighboring pixels in case 2 would be maintained to ensure the integrity of plots.

We employed the U-Net model to create the cashew plantation map for 2015 using aerial imagery. Each image tile was cut into image patches of 256 by 256 pixels before model training. The U-Net model has been prevalent in the crop classification domain (Kumar and Jayagopal, 2021; Wei et al., 2019; Zou et al., 2021) because of its advantages for segmentation tasks, including the combined use of global location and context, fewer training samples, and good performance (Alom et al.,

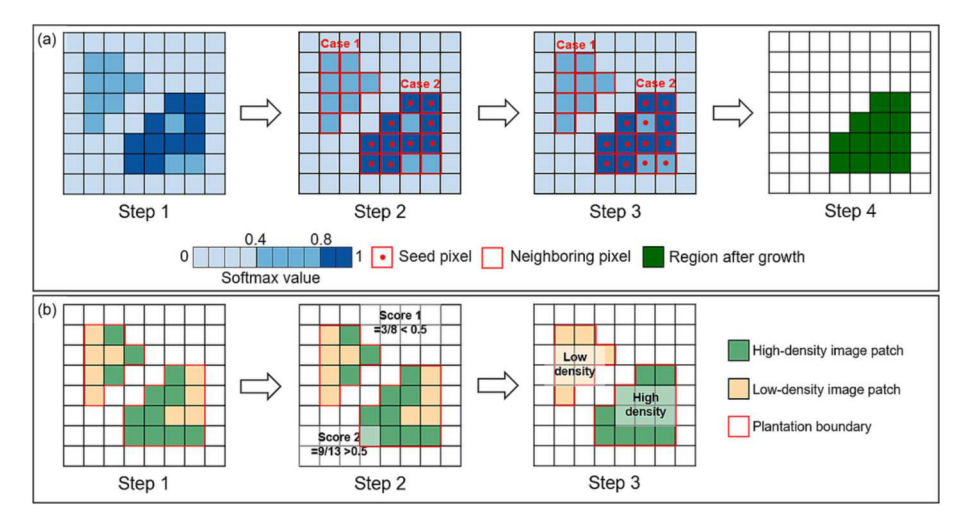


Fig. 4. (a) Region growing strategy and (b) the pathway to distinguish between high-density and low-density cashew plantations.

2018; Ronneberger et al., 2015). The same Monte Carlo dropout method was applied to create an average over ten predictions and express the prediction uncertainty. In this study, we used five convolution layers with the kernel of 3 by 3 pixels. Maxpool and transposed convolution layers were employed with the kernel of 2 by 2 pixels. The dropout rate is set to 0.3. Then, the region growing strategy was applied to produce the final cashew plantation map for 2015.

2.4.2.3. Classification post-processing. Based on the fact that perennial cashew plantations are not cut down once planted in our study region, the cashew plantation area identified in 2015 was used as a mask in the 2019, 2020, and 2021 classification maps to avoid omission errors. Similar masks were generated for 2019 and 2020 to identify cashew plantations over the years that followed. Given the fair classification performance for the built-up land class due to limited training labels, we used the land cover maps published in 2016 (ESA, 2017) and 2020 (ESA, 2021) by ESA to create masks for built-up land to update the classification result.

2.4.3. Mapping cashew planting density in plantations (tree-spacing practices)

Collecting tree planting density data at a national scale is a difficult task requiring a large commitment of time and resources, whether through visual interpretation of high-resolution images or on-site data collection, which renders the cost of supervised learning relatively high. Therefore, we need a learning strategy to categorize plantations into high- or low-planting density without the need for labels. Clustering is one such widely used unsupervised learning strategy; however, directly clustering the spectral bands of mono-temporal remote sensing imagery can lead to suboptimal results for several reasons. First, the clustering using spectral values at the pixel level can be noisy due to the spatial noise of the sensors. Second, clustering using all spectral values of all the pixels in an image patch can lead to very high dimensions and thus lead to issues like correlated attributes and inaccurate calculated distances. Third, multi-temporal remote sensing imagery includes more information to depict cashew tree crops than mono-temporal imagery. To address these challenges, we extracted abstract features - embedding from the satellite imagery time series using a spatiotemporal autoencoder and applied the clustering method at the embedding level. Furthermore, the traditional K-means clustering method (MacQueen, 1967) struggles with complicated imagery datasets (Xie et al., 2016), and it likewise fared poorly in our task. Therefore, we adopted a deep embedded clustering method (Xie et al., 2016) as our clustering method, which optimized the K-means result and thus improved our clustering performance (Ghosh et al., 2022).

In this study, the Clustering Augmented Self-supervised Temporal Classification (CASTC) model was leveraged to distinguish two kinds of cashew plantation tree-spacing practices (high-density versus lowdensity cashew plantations) using the temporal Planet Basemaps in 2021. Specifically, the encoder and decoder parts in the autoencoder structure have a similar architecture to STCA without the skip connections. Removing skip connections can help the model to extract quality encoded spatiotemporal vectors - embedding - that fully capture representative features without the assistance from the skip connections. The embedding output by the encoder is fed into an LSTM-based sequence decoder that generates a sequence of vectors, and a convolutional decoder then reconstructs back the input time-series satellite imagery based on the vector sequence. Model training consists of two phases: the first phase involves model initialization, and the second phase is model refinement with optimized clustering objectives. In the first phase, the autoencoder generated the embeddings, which were then subjected to the K-means clustering algorithm to generate initial cluster centroids. In the second phase, the cluster centroids obtained from the first phase were refined by matching soft assignment to target distribution by Kullback-Leibler (KL) divergence (Joyce, 2011) minimization. The soft assignment measures the similarity between an embedding and a cluster centroid with the t-distribution (Van der Maaten and Hinton, 2008) to generate the probability of assigning the embedding to the cluster:

$$q_{ij} = \frac{\left(1 + \left|h(X_i; \theta_h) - M_j\right|^2 / \alpha\right)^{\frac{\alpha+1}{2}}}{\sum_{j=1}^{K} \left(1 + \left|h(X_i; \theta_h) - M_j\right|^2 / \alpha\right)^{\frac{\alpha+1}{2}}}$$
(5)

where q_{ij} is the probability of assigning the i^{th} embedding to the j^{th} cluster, $h(X_i; \theta_h)$ is the i^{th} embedding, M_j is the j^{th} cluster centroid, α is the degree of freedom, and K is the number of cluster centroids. To promote model learning from high-confidence embeddings, the target distribution was computed by skewing the soft assignment to drive the embedding i closer to the cluster j with highest q_{ij} :

$$p_{ij} = \frac{q_{ij}^2 / \sum_{i} q_{ij}}{\sum_{j=1}^{K} \left(q_{ij}^2 / \sum_{i} q_{ij} \right)}$$
(6)

Then, we matched the soft assignment to the target distribution by minimizing the KL divergence to refine cluster centroids and encoder:

$$KL = \frac{1}{N_t} \sum_{i=1}^{N_t} \sum_{j=1}^{K} p_{ij} log \left(\frac{p_{ij}}{q_{ij}} \right)$$
 (7)

where N_t is the number of image patches in the training set.

Before model training, each image tile was cut into image patches of 32 by 32 pixels. After training the model, we had ten clusters, and the model was used to assign a cluster for each image patch in the training set. For the image patches for each cluster, we then visually inspected the corresponding high-resolution Airbus satellite imagery and assigned the image patches as high density or low density (step 1 in Fig. 4(b)). We applied this model to the entire study region and kept only the cashew plantation region using a cashew plantation distribution mask. Each separate cashew plantation was given a density score from 0 to 1 (step 2 in Fig. 4(b)) to indicate the ratio of high-density image patches according to Eq. (4). Then, a density score threshold of 0.5 was applied to distinguish between high-density and low-density plantations (step 3 in Fig. 4(b)).

$$density\ score = \frac{N_{high-density-patches}}{N_{all-patches}}$$
(8)

2.4.4. Validation of cashew plantation classification maps

Two accuracy assessment methods were performed on the cashew plantation distribution in two dimensions: space and time. In the spatial dimension, we verified the accuracy for each year using 1400 ground truth samples. A confusion matrix, overall accuracy (OA), user's accuracy (UA), and producer's accuracy (PA) were used to evaluate the accuracy. In the time dimension, we verified the consistency of the classification results from 2015 to 2021 using 196 cashew plantation samples located in the same place across years. Note that built-up areas were ignored in our accuracy assessment, as this information was derived from existing products and was not the focus of this study. To assess the accuracy of cashew plantation tree-spacing practices, 348 points with known planting density were used.

2.4.5. Benchmarking with other classification approaches

The performance of STCA was compared with three deep learning methods: U-Net with 3D-CNN (Ji et al., 2018), U-Net with ConvLSTM (Ghosh et al., 2021; Shi et al., 2015), and CALD (Jia et al., 2019), all of which were designed to learn spatiotemporal information and have been shown to perform well in crop classification tasks. We did not include simple machine learning methods for comparison with STCA because they do not take spatial information into account in their classification, and the CALD approach has been shown to perform much better on cropland mapping than RF and SVM (Jia et al., 2019). Compared to the traditional CNN network, U-Net with 3D-CNN exploits additional temporal information by conducting convolution in the time dimension to learn temporal information. U-Net with ConvLSTM utilizes the U-Net architecture but substitutes the convolution layers with ConvLSTM layers, which can capture spatial and temporal information with CNN and LSTM. CALD leverages a context-aware LSTM to capture temporal information and further learn spatial information from neighboring pixels. We compared the classification performance of these four approaches within the training region. UA and PA were used to assess classification performance for each class.

We also compared the performance of CASTC with two other standard self-supervised classification methods, i.e., Autoencoder with K-means (Ghosh et al., 2022) and Colorization with K-means (Vincenzi et al., 2021). Autoencoder is a standard spatiotemporal STCA architecture without the skip connections. Colorization is a self-supervised learning technique with two independent branches taking in the NIR and RGB channels. Both of the branches are trained by the autoencoder separately, and we averaged their respective embeddings from the final layer as final embeddings. K-means is performed on the embeddings from the final layer of the encoder for both methods. To compare the clustering performance of the three approaches at the embedding level,

we measured the inter- and intra-cluster differences using two metrics, the Separability Index (SI) and Coefficient of Variation (CV). SI (Somers and Asner, 2013) was used to measure the inter-class difference (Eq. (9)):

$$SI_{i,j} = \frac{|\mu_i - \mu_j|}{\sigma_i + \sigma_i} \tag{9}$$

where i and j represent different embedding clusters; μ_i and μ_j refer to the mean value of cluster i and cluster j, respectively; σ_i and σ_j represent the standard deviation of cluster i and cluster j, respectively. The numerator can reflect the disparity between different clusters, while the denominator can indicate the degree of concentration within clusters (Hu et al., 2019; Yin et al., 2020). A larger SI indicates greater dissimilarity between the embeddings in the two clusters. CV was used to measure intra-cluster differences, and it is unitless (Eq. (10)):

$$CV_i = \frac{\sigma_i}{\mu_i} \tag{10}$$

where i represents a cluster, and σ_i and μ_i refer to the mean value and standard deviation of a cluster, respectively. A smaller CV indicates a greater concentration of embeddings in the cluster. Then, we compared the distribution of SI and CV for the three approaches.

2.4.6. Comparison of classification performance between Planet Basemaps, Planet Daily Scenes, and Sentinel-2 L2A product

To explore the gain from Planet Basemaps that results from higher spatial resolution and less cloud cover, we compared the classification performance with the STCA model for the Sentinel-2 L2A product (four bands and ten bands), Planet Daily Scenes, and Planet Basemaps in the training region. For each product, monthly composite from Nov. in 2019 to May in 2020 were input into the STCA model. To evaluate the benefits of more spectral information, two variations of Sentinel-2 L2A products were utilized for comparison – one encompassing four bands (RGB + NIR) and the other with ten bands (four red-edge bands and two shortwave infrared bands in addition to the initial four bands).

3. Results

3.1. Results of benchmark experiments

Fig. 5 presents a detailed visual comparison of classification results in eight spots across four scenarios/sites. For spot a in site 1, only the STCA model accurately classified cashew plantations and preserved the border integrity of the plantation. The other three models misclassified cashew plantations as mixed trees/grassland. The STCA model performed the best in site 1. For spot b in site 2, both STCA and U-Net ConvLSTM correctly classified cashew plantations with relatively sparse trees, while the other two models misclassified them as cropland/others. For spot c, CALD and STCA accurately classified cropland/others, while the other two models misclassified them as mixed trees/grassland. The STCA model performed the best in site 2. For the spots of d, e, and f in site 3, both STCA and U-Net_ConvLSTM accurately classified more cashew planting areas than the other two models. For spot g in site 4, STCA and U-Net_3D-CNN demonstrated superior classification performance for cashew plantations, while CALD and U-Net ConvLSTM misclassified them as mixed trees/grassland. For spot h, STCA's border delineation for cashew plantations best matched the label. In summary, the STCA model consistently provided the best classification results across all four sites, showcasing stable performance. It effectively delineated cashew plantation borders and maintained plantation integrity by automatically focusing on the most significant time steps for classification performance and incorporating the region growing method. The CALD model exhibited the poorest performance due to insufficient spatial information capture, resulting in more errors at individual pixels. Both U-Net_3D-CNN and U-Net_ConvLSTM demonstrated better classification

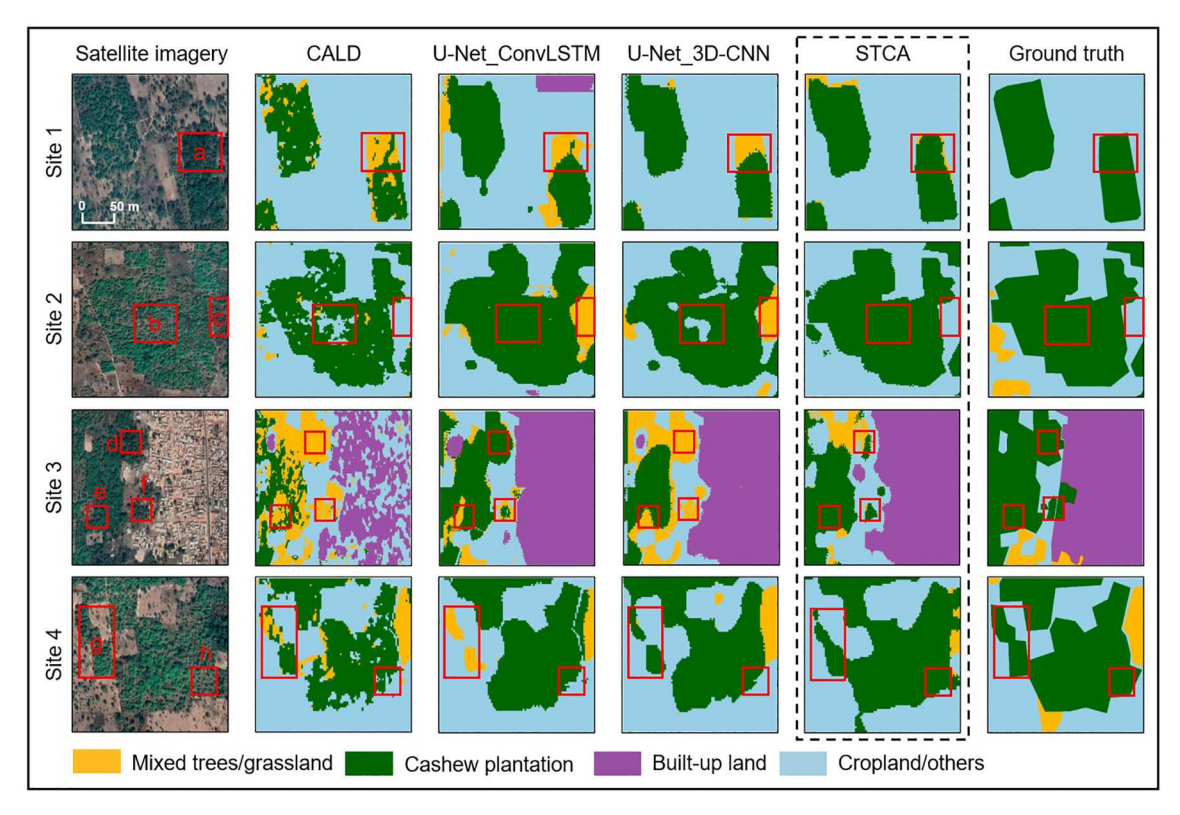


Fig. 5. Classification results for STCA and baselines along with ground truth labels and high-resolution satellite imagery from Google Earth. Eight spots (red frames a-h) show local details of different classification results. (For interpretation of the references to colour in this figure legend, the reader is referred to the web version of this article.)

abilities than CALD, although they could not identify the most contributory time steps.

Table 2 shows the classification performance statistics for the four different models and supports the visual comparison in Fig. 5. For the cashew plantations, the STCA classification result reached 85% PA and 83% UA, while the PA and UA of the other three methods were below 80%, with CALD performing the worst. This indicates that STCA produced fewer omissions and misclassifications of cashew plantations. Although all four models achieved over 80% PA and UA for the mixed trees/grassland class, STCA had fewer omissions. For the cropland/others class, the STCA method exhibited the highest PA and UA, indicating it accurately classified the most pixels and omitted the fewest pixels for this class.

Fig. 6(a) illustrates the classification comparison between CASTC and the two other benchmark self-supervising approaches. In terms of Separability Index (SI), a measure of inter-class difference, although CASTC has a slightly lower median value than Colorization with K-means, the first quantile and the maximum are noticeably higher, which

Table 2
Accuracy assessment for STCA and benchmark methods.

Methods	CALD	U- Net_ConvLSTM	U-Net_3D- CNN	STCA
PA/UA				
Mixed trees/grassland (PA)	81.6%	82.4%	83.5%	88.1%
Mixed trees/grassland (UA)	82.3%	83.2%	81.9%	84.4%
Cashew plantation (PA)	75.1%	77.2%	78.4%	85.7%
Cashew plantation (UA)	76.3%	78.5%	77.2%	83.0%
Built-up Land (PA)	63.4%	65.5%	58.3%	70.4%
Built-up Land (UA)	50.7%	55.9%	60.7%	65.5%
Cropland/others (PA)	68.3%	70.4%	74.8%	80.2%
Cropland/others (UA)	72.3%	73.6%	69.6%	84.7%

indicates much greater divergence of some cluster pairs. Autoencoder with K-means has the poorest clustering performance. In the comparison of Coefficient of Variation (*CV*), a measure of intra-class difference, the maximum and median of CASTC are the lowest among the three methods, although the minimum is slightly higher than Colorization with K-means. Colorization with K-means has the greatest median and maximum values of the three approaches, indicating that more than half of the clusters it formed were highly dispersed. As shown in Fig. 6(b), the image patches from two clusters formed by CASTC show obvious differences in cashew tree density. High-density clusters stand out in sharp contrast to low-density clusters. However, for Autoencoder and Colorization with K-means, high-density and low-density cashew plantations are mixed in the same cluster, indicating that the two methods perform poorly in this task.

3.2. Accuracy assessment for cashew plantation distribution and plantation density

The individual OA values of the cashew plantation maps are 0.89 ± 0.0186 , 0.87 ± 0.0187 , 0.85 ± 0.0204 , and 0.90 ± 0.0164 for 2015, 2019, 2020, and 2021, respectively, (Table S2 and Table S4–6) with 1400 validation points. The cropland/others class was most frequently misclassified with cashew plantations. A small amount of mixed trees/grassland labels were also found in points predicted to be cropland/others. The greater UA of cashew plantations for 2019, 2020, and 2021 than in 2015 was expected, given that no temporal information could be used for the mono-temporal imagery. We also checked the resampled 2.4-m cashew map in 2015, which shows very similar OA, UA, and PA for each category (Table S2 and Table S3). Given the higher spatial resolution, we retained the 0.5-m cashew map for further analysis. In terms of classification consistency, 83.7% of the samples were consistently classified as cashew plantation across the years, which demonstrated the stability of the classification along the time dimension

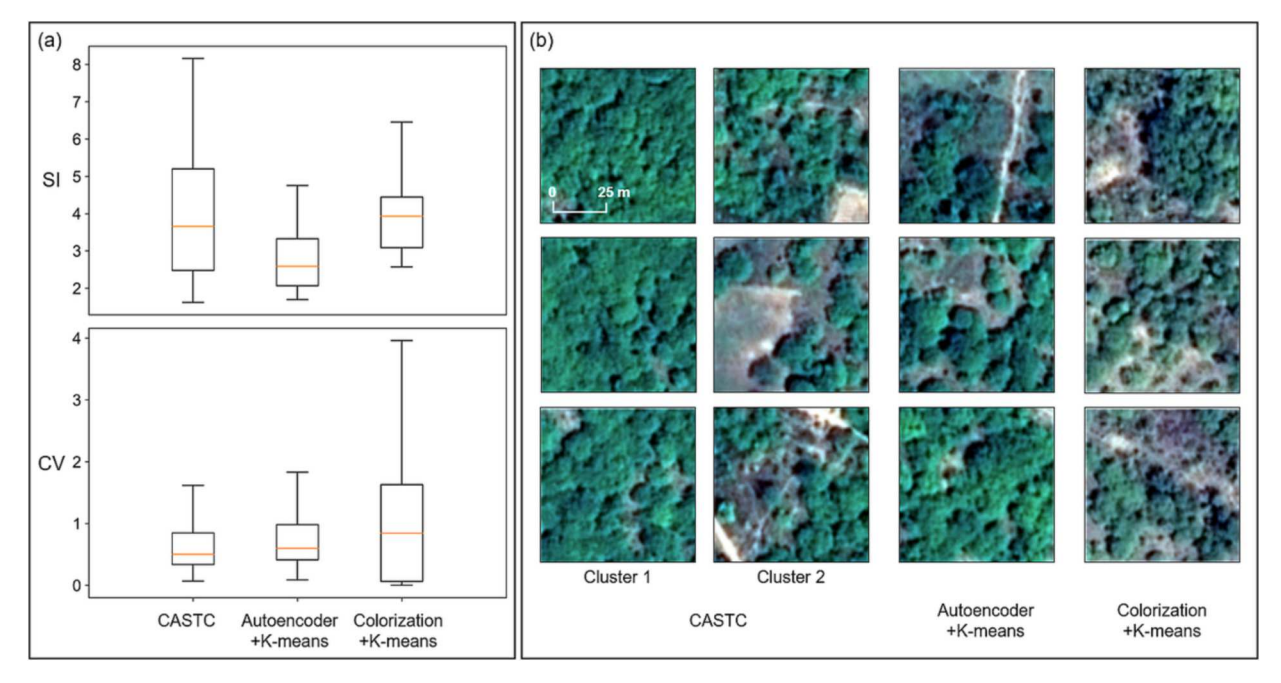


Fig. 6. (a) Comparison of clusters generated by CASTC and benchmark methods by (a) Separability Index (SI) and Coefficient of Variation (CV). (b) The results generated by CASTC exhibited a more consistent cashew tree planting density compared to Autoencoder with K-means and Colorization with K-means.

(Table S7). The OA for cashew plantation density mapping was 0.76 \pm 0.0492 (Table S8). Low-density cashew plantations were better categorized than high-density plantations, possibly because the number of high-density plantation samples, 128, was smaller than that of low-density samples, 220. We also would like to note that 18.6% of high-density plantations with small crowns were misclassified as "low-density cashew plantation" in newly developed cashew plantations between 2015 and 2021.

3.3. Spatial distribution of cashew plantations in 2021

Fig. 7 shows the distribution of cashew plantations in 2021, and Table 3 summarizes the cashew plantation area and share of land planted with cashew trees in 2021 for each commune. The area of cashew plantations in 2021 is 519 ± 20 thousand hectares (kha). The Bantè commune has the greatest share of land dedicated to cashew plantations, with nearly 300 ha of plantations per kha land, while two

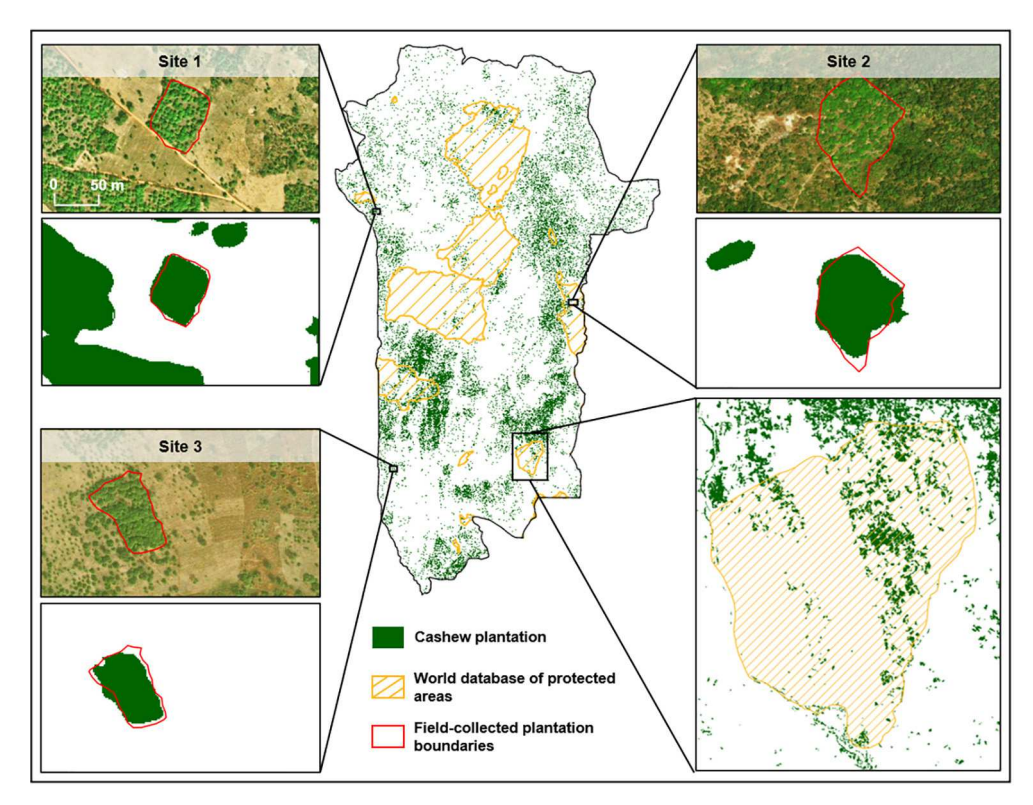


Fig. 7. The distribution of cashew plantations in 2021. Three sample sites are shown with classification maps and satellite imagery from Google Earth.

Table 3Total cashew area and share of land planted with cashew trees for communes as of 2021.

Metrics Cashew area (kha)		Share of land planted with cashew trees (ha/kha)					
Communes							
N'Dali	35 ± 6	90 ± 15					
Parakou	7 ± 1	149 ± 21					
Tchaourou	102 ± 7	140 ± 10					
Bantè	79 ± 4	299 ± 15					
Dassa- Zoumè	20 ± 5	114 ± 28					
Glazoué	23 ± 5	142 ± 28					
Ouèssè	43 ± 6	174 ± 19					
Savalou	46 ± 7	197 ± 26					
Savè	51 ± 6	128 ± 26					
Bassila	40 ± 5	40 ± 10					
Djougou	29 ± 4	73 ± 10					
Djidja	35 ± 9	199 ± 43					

other communes (Savalou and Djidja) have nearly 200 ha of cashew plantations per kha land. Djougou, N'Dali, and Bassila communes have <100 ha cashew plantations per kha land. The Tchaourou has the greatest total cashew plantation area with 102 ± 7 kha, and accounts for nearly one fifth of total cashew plantation area in Benin. Additionally, we found that cashew plantations have encroached on 45 ± 6 kha of protected areas, using boundaries in Benin within the World Database of Protected Areas (WDPA). 55% more protected area has been encroached upon by cashew plantations in 2021 than in 2015 (29 \pm 7 kha). The

online version of the cashew plantation map is available on TechnoServe Lab (https://cajuboard.tnslabs.org).

3.4. Cashew plantation expansion from 2015 to 2021

The classification results for the four years indicate that the area of cashew plantations almost doubled from 268 \pm 15 kha to 519 \pm 20 kha between 2015 and 2021. This confirms public statistics from the Benin Ministry of Agriculture, Livestock and Fisheries that the area under cultivation increased by 71% from 286 kha in 2016 to 488 kha in 2020 (MAEP-Benin, 2020). During the last seven years, there were clear signs of growth in west and east Collines, west Donga, and south Zou, as shown in Fig. S2. Fig. 8(a) quantitatively shows the composition of the original land cover type from which the new cashew plantations were established. The departmental statistics show that the cashew plantation area increased in all four departments over the past seven years with the highest growth in Collines and the lowest growth in Zou. From 2015 to 2021, the cropland/others class accounted for more cashew expansion than the mixed trees/grassland class for all four departments. Only in two instances - in Borgou and Zou between 2015 and 2019 - did conversion to cashew plantations from mixed trees/grassland exceed 50%. The highest conversion from mixed trees/grassland to cashew plantations occurred in Borgou from 2015 to 2019 with 58.3% cashew expansion, while the lowest occurred in Zou from 2020 to 2021, with 23.4% cashew expansion.

The statistics of the same metrics are provided for each commune in Fig. 8(b). All 12 communes had continuous cashew expansion over the last seven years. The highest cashew plantation area growth occurred in

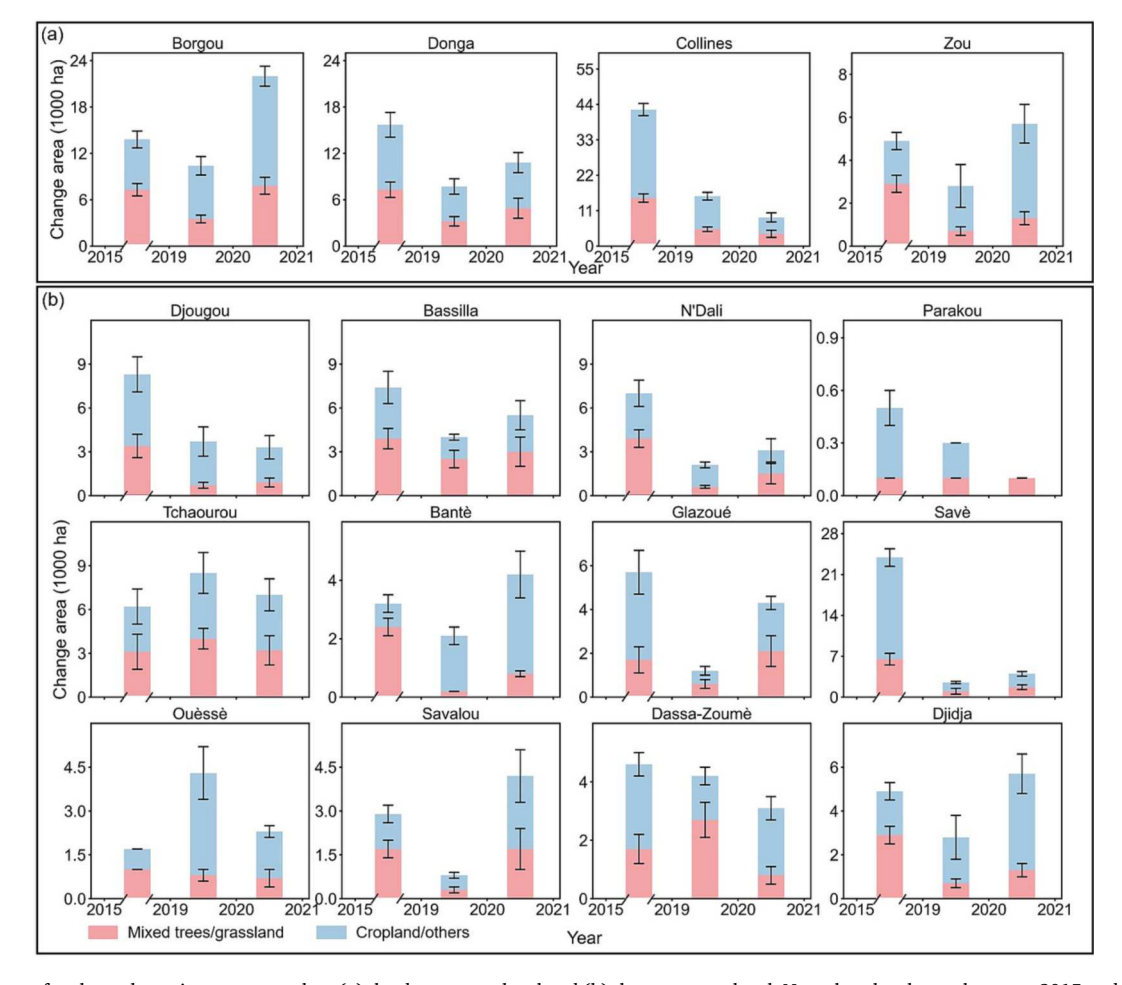


Fig. 8. The source of cashew plantation area growth at (a) the department level and (b) the commune level. Note that the change between 2015 and 2019 represents a larger time increment on the x-axis than between individual years.

Savè, while the lowest growth occurred in Parakou, likely because the area of Parakou is smallest among the 12 communes and space for establishing new cashew plantations is very limited. The relative conversion of mixed trees/grassland and cropland/others to cashew plantations varies greatly from region to region. Between 2015 and 2019, more mixed trees/grassland than cropland/others were converted to cashew plantations in Bantè, Ouèssè, Savalou, Djidja. Two such individual changes also occurred each between 2019 and 2020 (Bassilla and Dassa-Zoumé) and between 2020 and 2021 (Bassilla and Parakou). For other periods and communes, the cropland/others class accounted for more cashew expansion than mixed trees/grassland.

3.5. Planting density map of cashew plantations for 2021

The map of cashew plantation planting density scores is shown in Fig. 9(a). A threshold planting density score of 0.5 was selected to distinguish high-density and low-density cashew plantations (Fig. 9(b)), and details are shown for three sample sites in Fig. 9(c). As shown in Fig. 9(d), the proportion of high-density cashew plantations relative to the total reveals that 5 communes significantly exceed 50%, namely N'Dali, Tchaourou, Bantè, Ouèssè, and Savalou. These five communes are all located in the Borgou and Collines departments, which means these two departments, especially Borgou, have a relatively mature

cashew cultivation industry. On the other hand, although the three communes of Glazouè, Bassilla, and Djougou have relatively large cashew plantation areas, the tree density is low, which presents an opportunity to increase cashew planting density (and therefore cashew production) on existing plantations.

4. Discussion

4.1. The added value of Planet Basemaps in large-scale smallholder crop mapping

Although some previous studies have focused on smallholder crop mapping, the limited spatial and temporal resolution of the available remote sensing data was not adequate for creating field-level maps. Prior to the Sentinel mission launch, Landsat and MODIS data were used to map smallholder farms (Jain et al., 2013; Schneibel et al., 2017). Later, Sentinel-1/2 were widely used for crop functional mapping of all kinds, especially in Africa (Jin et al., 2019; Lambert et al., 2018; Masiza et al., 2020). However, the highly fragmented fields and frequent cloud coverage in some small regions can cause satellite imagery with medium spatial/temporal resolution to lose its efficiency. Sentinel-2 imagery cannot adequately depict smallholder cashew plantation field boundaries, given its insufficient spatial and temporal resolution and the

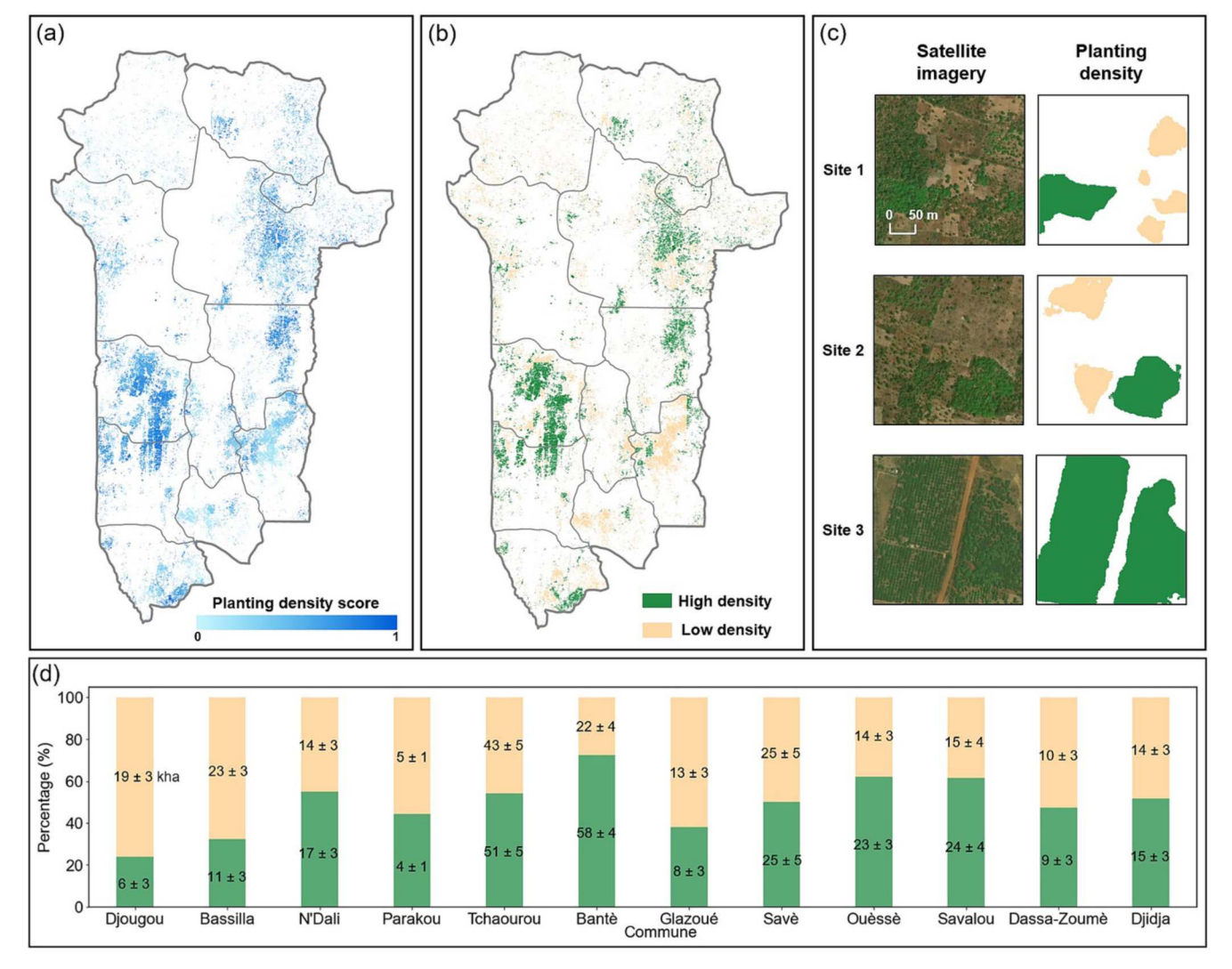


Fig. 9. (a) A map of cashew plantation planting density scores in 2021. (b) A map of high- and low-density cashew plantations in 2021 with a threshold of 0.5. (c) Three sample regions with high- and low-density cashew plantations. The high-resolution satellite imagery is from Google Earth. (d) The percentage and area of high- and low-density cashew plantations for all communes.

degradation of image quality by clouds and shadows (Fig. S3(a)). Recently, researchers have realized the advantages of the high spatial and temporal resolution in Planet's microsatellite constellation for crop mapping. Some promising smallholder crop mapping results using Planet Daily Scenes SR data (3 m) have been published, although they typically consist of small-scale (< 1000 km²) applications (Rafif et al., 2021; Rao et al., 2021). However, such daily images are still affected by clouds and shadows to varying degrees (Fig. S3(b)). In comparison, Planet Basemaps generally contain less noise (Fig. S3(c)). This is because the monthly Planet Basemaps go through more post-processing steps than Planet Daily Scenes, as mentioned in Section 2.2.1 and 2.2.3. To summarize, Planet Basemaps enable field-specific, and even sub-field, crop monitoring.

Fig. 10 shows the classification performance for the Planet Basemaps, Planet Daily Scenes, and Sentinel-2 L2A product. The classification outcome utilizing four bands (RGB + NIR) from the Sentinel-2 L2A product frequently misidentified cashew plantations as mixed trees/ grassland and cropland areas, whereas the result employing ten bands approximated the outline more accurately, as exemplified by sites 1 and 2 in Fig. 10, due to the inclusion of six additional bands. The classification derived from Planet Daily Scenes exhibited enhanced boundary delineation compared to Sentinel-2, attributable to its superior spatial resolution. Nonetheless, daily images remain susceptible to cloud and shadow interference, occasionally leading to confusion between cashew trees and mixed trees/grassland, as demonstrated by sites 1 and 3. In contrast, Planet Basemaps yielded more accurate classifications of cashew plantations due to its enhanced spatial resolution and reduced cloud interference. The classification accuracy assessment using F1 scores further indicates that Planet Basemaps produced superior classification results compared to the other three data sources (Table 4). For cashew plantations, the classifications based on the 10-band Sentinel-2 L2A product and Planet Daily Scenes both achieved approximately 80% accuracy, whereas Planet Basemaps achieved 84% accuracy. This suggests that increased spectral information can partially compensate for coarser spatial resolution. The advantages offered by current and forthcoming satellite data with more spectral information, such as Sentinel-2, Landsat Next super-spectral satellites (NASA Landsat Next, 2022), and ESA's CHIME hyperspectral satellites (Nieke and Rast, 2018), along with data fusion approaches (Ghamisi et al., 2019; Liu

Table 4Accuracy assessment for Sentinel-2 L2A, Planet Daily Scenes, and Planet Basemaps using F1 scores.

Products	Sentinel-2 L2A (4 bands)	Sentinel-2 L2A (10 bands)	Planet Daily Scenes	Planet Basemaps	
Class					
Mixed trees/ grassland	0.7471	0.7918	0.8535	0.9103	
Cashew plantation	0.6723	0.8032	0.7941	0.8410	
cropland/others	0.6837	0.7719	0.7529	0.7830	

et al., 2022; Tang et al., 2021; Zhou et al., 2021) that combine the strengths of high spatial and spectral resolution, offer promising avenues worth exploring for smallholder tree crop mapping in future studies.

4.2. Uncertainty analysis of classification results

Because the study region is located in the tropics, clouds and shadow weaken the observational capability of optical sensors. At the same time, the Planet microsatellite constellation consists of many satellites, which inevitably causes differences in sensor characteristics, thus affecting the ability to obtain consistent SR for a large region to some extent. Additionally, other factors such as satellite product versions, atmospheric and directional corrections, and BRDF effects can also cause classification uncertainty (Zeng et al., 2022). All of these factors not only have impacts on the direct monitoring ability for cashew plantations, but also introduce inter-class similarity and intra-class differences, resulting in poor classification performance. In order to explore the impacts of these factors on the classification results, we employed an uncertainty mask generated by the Monte Carlo dropout technique (Eq. (4)) to filter out the pixels impaired by these factors. Fig. 11(a) shows the real surface conditions with satellite imagery. The pixel-wise classification uncertainty mask from ten runs with Monte Carlo dropout (Fig. 11(c)) was applied to the averaged classification results of the ten runs (Fig. 11(b)) with a threshold of 0.06 to generate a cashew plantation map without high-uncertainty pixels (Fig. 11(d)). The threshold can be adjusted case by case.

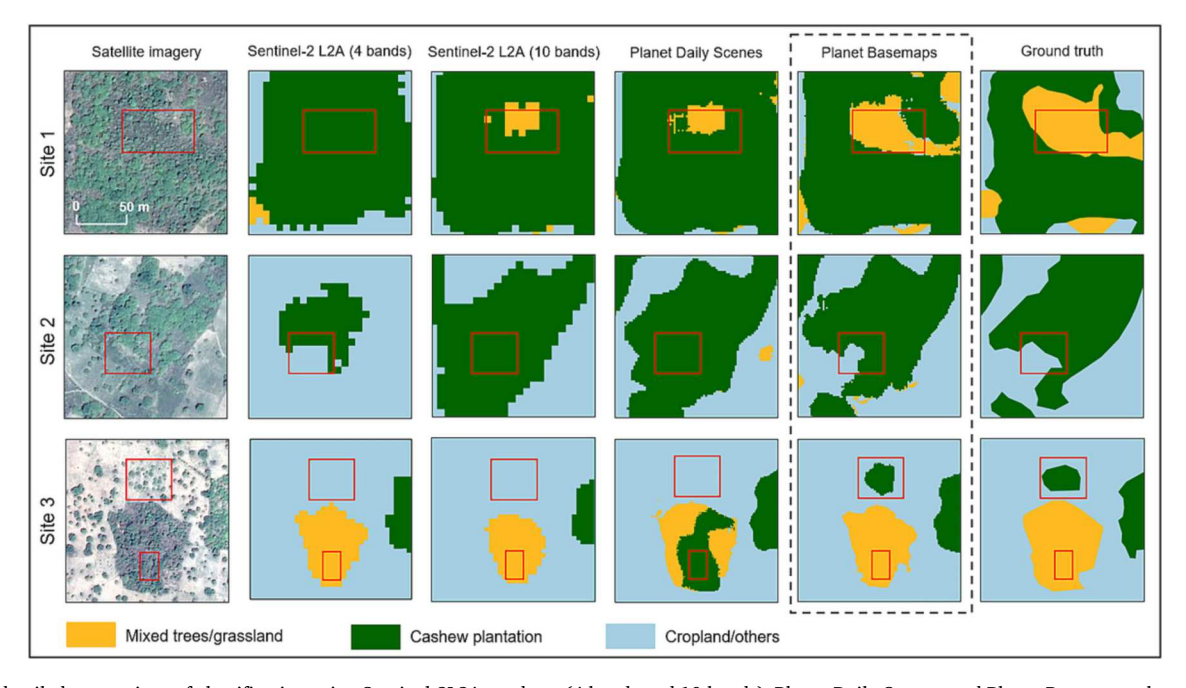


Fig. 10. A detailed comparison of classification using Sentinel-2L2A products (4 bands and 10 bands), Planet Daily Scenes, and Planet Basemaps, shown along with Airbus satellite imagery and ground truth labels.

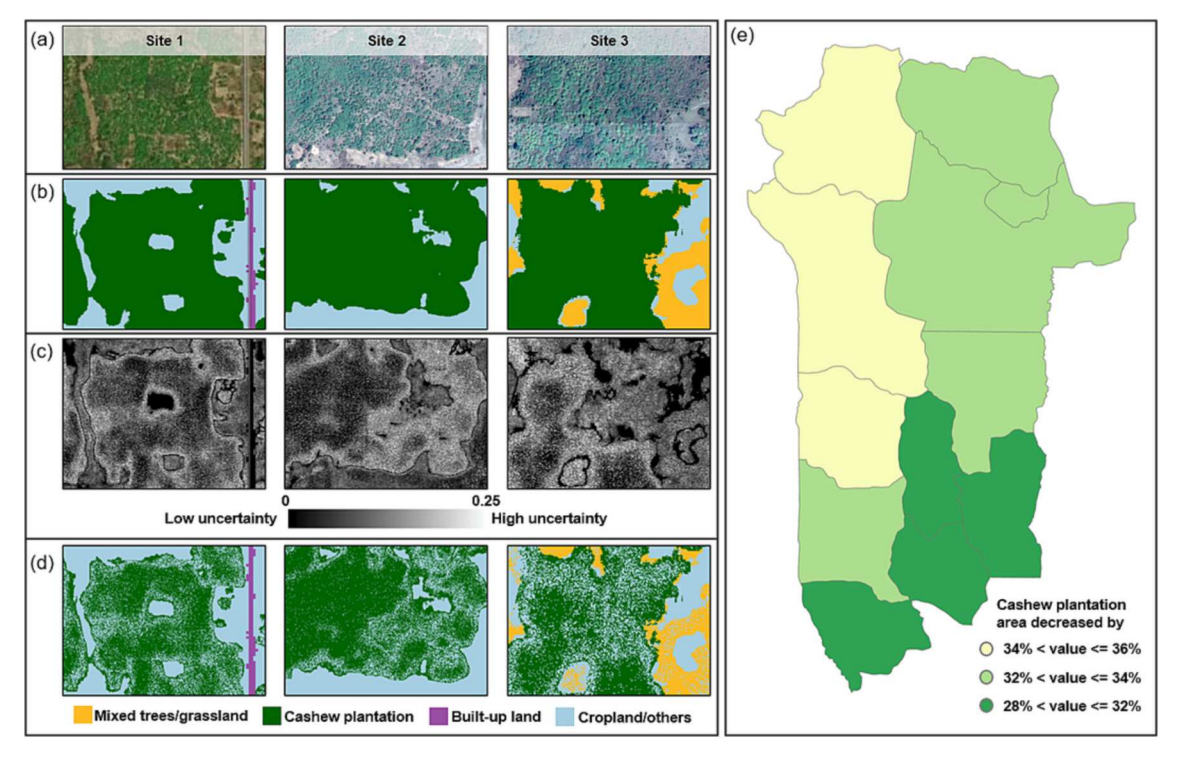


Fig. 11. A process to generate a cashew plantation map without high-uncertainty pixels. (a) Airbus/Maxar satellite imagery with 0.5-m resolution. (b) Classification map. (c) Uncertainty map. (d) The classification map masked by the uncertainty map with a threshold equal to 0.06. I Cashew area changes compared with the original classification map for each community after applying the uncertainty mask for 2021.

We took the classification result in 2021 as an example and divided the study region into three parts based on the degree of cashew plantation area decline after applying the uncertainty mask (Fig. 11(e)). Communes are relatively spatially concentrated for each class. There are four communes in the southeast of the study region that experienced less decline than other communes (i.e., Djidja, Dassa-Zoumè, Savè, and Glazoué) among which Savè declined the least. On the other hand, the three northwestern communes of Djougou, Bassila, and Bantè declined more than other communes, among which Bassila declined the most.

4.3. Policy guidance for the cashew industry in Benin

The findings of this study help document the progress of a major governmental initiative known as the Strategic Plan for the Development of the Agricultural Sector (PSDSA). A key goal under this plan was to double cashew production from 112,000 metric tons to 200,000 metric tons from 2016 to 2021 (MAEP-Benin, 2017). The results produced here provide additional inputs to inform the PSDSA for 2022–2025 (PNIASAN-Benin, 2022).

First, we tracked the increase in cashew areas under cultivation from 2015 to 2021. Our modeling shows that Benin increased cashew plantations from 268 \pm 15 kha to 519 \pm 20 kha between 2015 and 2021, which is very close to the government estimate of 286 kha under cultivation as of 2016 and 488 kha as of 2020 (MAEP-Benin, 2020). In 2021, Tchaourou had the largest cashew area (102 \pm 7 kha) in 12 communes, and Parakou had the lowest (7 \pm 1 kha). 60% of new cashew plantations came from lands that were previously under crop production or left fallow. According to the boundary of WDPA, the area of cashew plantations within protected areas grew from 29 \pm 7 kha to 45 \pm 6 kha between 2015 and 2021, an increase of 55%.

We further explored the overall planting density of cashew plantations based on the 2021 classification map. To increase cashew nut yield, it is important to implement good agricultural practices and to increase tree-planting density in areas we have classified as low-density. Our result shows that for the communes N'Dali, Tchaourou, Bantè, Ouèssè,

and Savalou, most of the cashew plantation area is high-density. However, for the communes Djougou, Bassila, and Glazoué, most cashew plantations are low-density. In our study region, over 90% of new cashew plantations established between 2015 and 2021 were low-density. Increased application of inputs (seedlings) in low-density cashew plantations coupled with targeted training efforts in all cashew growing areas that have not yet received training could have a significant impact on cashew nut yields.

4.4. Limitations and future work

The combination of tree crop classification algorithms for cashew and high-resolution imagery demonstrated the power of accurately mapping the distribution and planting density of cashew plantations, upon which we monitored the dynamics of cashew areas under cultivation from 2015 to 2021. The proposed classification algorithms will allow rapid mapping of cashew plantations going forward. However, some limitations remain to be optimized in the future. First, because of a small amount of missed clouds and shadows during image selection and differences in sensor characteristics of the satellite constellation, intraclass spectral inconsistency is still an issue for some regions, even after Planet Basemaps have been normalized to the Sentinel-2-based seasonal model. Some cashew plantations were consequently omitted, requiring a mask during postprocessing to include omitted cashew plantations on an annual basis. This challenge is common in the remote sensing field, and solutions are limited. A potential method is using domain adaptation, including invariant feature selection, representation matching, adaptation of classifiers, and selective sampling (Elshamli et al., 2017; Martini et al., 2021; Tuia et al., 2016). Recently, the new generation of Planet-Scope instruments with 4 newly added bands (coastal blue, yellow, a second green, and red edge spectral bands) has launched and started publishing imagery (Planet, 2022d). The new analytic product is calibrated to Sentinel-2 and has improved alignment, enabling accurate time-series analysis and machine learning models (Planet, 2022e). In future classification map updates, domain adaptation algorithms and the next generation of PlanetScope instruments will contribute to further improving the accuracy of cashew plantation maps and reducing the support from the mask during postprocessing. Second, although the 2.4m Planet Basemaps were leveraged to distinguish high- and low-density cashew plantations using the threshold value of 100 trees/ha, remote sensing imagery with higher spatial resolution can help differentiate additional levels of planting density (e.g., "very-high-density" plantations above 180 trees/ha) as a result of finer observational ability. For those newly developed high-density plantations with small crowns misclassified as "low-density cashew plantation", capturing finer texture details using higher-resolution images would also prove advantageous in reducing the misclassification. This is because high-density plantations with small crowns are often well-organized in neat rows, while the actually low-density plantations are more likely to plant trees randomly (Fig. S4). In addition, more information about GAP adoption in cashew plantations can be captured, such as whether trees are pruned (i.e., tree crowns are not touching each other), which is important for improving cashew tree yields. In the future, more agricultural practices will be mapped.

With further work and close coordination between researchers and field teams, we will geographically expand the modeling techniques in this study to other cashew growing regions, and then to other major smallholder tree crops such as mango, avocado, shea, and macadamia, helping to improve the livelihoods of millions of smallholder farmers globally. In addition, based on tree crop maps, we can further understand the contribution of tree crops to carbon stocks and the benefits of expanding tree crop planting area for carbon sequestration, which could complement the research on the role of non-forest trees in mitigating climate change (Brandt et al., 2020; Mugabowindekwe et al., 2022; Skole et al., 2021).

5. Conclusion

In this study, we mapped the spatial distribution of cashew plantations from 2015 to 2021 and cashew planting density in 2021 with our developed tree crop mapping algorithms. Combining high-resolution Planet Basemaps and aerial imagery, even with limited ground truth labels, the STCA and U-Net showed promising performance in mapping cashew plantation locations in each of the four years. The methods and data sources used allowed us to achieve this result even in the face of difficult challenges that included heterogeneous landscapes and irregularly-planted smallholder farms, similar spectral signatures between cashew and other trees, pervasive and year-round clouds and shadows, and frequent land-use changes. We found that cashew plantation areas in Benin almost doubled since 2015 from 268 \pm 15 kha to 519 ± 20 kha in 2021. With the self-supervised learning model CASTC, the cashew plantation planting density map provided important information to assist in identifying regions with the greatest need for guidance on tree-spacing practices. Besides, the Planet Basemaps were demonstrated as a credible data source in classifying smallholder tree crops. Moving forward, the integration of high spatiotemporal resolution from Planet images with enhanced spectral information from diverse sources (e.g., Landsat Next super-spectral satellites and CHIME hyperspectral satellites) presents prospective avenues meriting exploration for smallholder tree crop mapping. Although the tree crop classification algorithms in this study were designed for mapping cashew plantations in Benin, they can be adapted in the future for other cashew growing regions and to map the distribution and planting density of other smallholder tree crops.

CRediT authorship contribution statement

Leikun Yin: Conceptualization, Methodology, Software, Investigation, Writing – original draft. **Rahul Ghosh:** Methodology, Software, Writing – review & editing. **Chenxi Lin:** Methodology, Investigation, Writing – review & editing. **David Hale:** Conceptualization,

Methodology, Resources, Investigation, Writing – review & editing. Christoph Weigl: Resources, Investigation, Writing – review & editing. James Obarowski: Resources, Writing – review & editing. Junxiong Zhou: Writing – review & editing. Jessica Till: Writing – review & editing. Xiaowei Jia: Methodology, Writing – review & editing. Nanshan You: Writing – review & editing. Troy Mao: Writing – review & editing. Vipin Kumar: Methodology, Writing – review & editing. Zhenong Jin: Conceptualization, Methodology, Resources, Investigation, Writing – review & editing.

Declaration of Competing Interest

The authors declare that they have no known competing financial interests or personal relationships that could have appeared to influence the work reported in this paper.

Data availability

Data will be made available on reasonable request.

Acknowledgements

This research is supported by BeninCajù Program of TechnoServe, a project funded by United States Department of Agriculture (USDA) – Foreign Agricultural Service (FAS). The authors acknowledge Seth Ayim and Martin Boton for their early assistance in field ground truth collection and dissemination, Yufeng Yang for helping annotate ground truth labels, and Joe Kington from Planet company for clarifying further details on the Planet Basemaps generation pipeline.

Appendix A. Supplementary data

Supplementary data to this article can be found online at https://doi. org/10.1016/j.rse.2023.113695.

References

- Alom, M.Z., Hasan, M., Yakopcic, C., Taha, T.M., Asari, V.K., 2018. Recurrent residual convolutional neural network based on u-net (r2u-net) for medical image segmentation. arXiv preprint arXiv:1802.06955.
- Alzubaidi, L., Zhang, J., Humaidi, A.J., Al-Dujaili, A., Duan, Y., Al-Shamma, O., Santamaría, J., Fadhel, M.A., Al-Amidie, M., Farhan, L., 2021. Review of deep learning: concepts, CNN architectures, challenges, applications, future directions. J. Big Data 8, 1–74.
- Atzberger, C., 2013. Advances in remote sensing of agriculture: context description, existing operational monitoring systems and major information needs. Remote Sens. 5, 949–981.
- Ballester-Berman, J.D., Rastoll-Gimenez, M., 2021. Sensitivity analysis of Sentinel-1 backscatter to oil palm plantations at pluriannual scale: a case study in Gabon, Africa. Remote Sens. 13, 2075.
- Basso, B., Liu, L., 2019. Chapter four seasonal crop yield forecast: methods, applications, and accuracies. In: Sparks, D.L. (Ed.), Adv. Agron. Academic Press, (201–255).
- Becker-Reshef, I., Justice, C., Barker, B., Humber, M., Rembold, F., Bonifacio, R., Zappacosta, M., Budde, M., Magadzire, T., Shitote, C., Pound, J., Constantino, A., Nakalembe, C., Mwangi, K., Sobue, S., Newby, T., Whitcraft, A., Jarvis, I., Verdin, J., 2020. Strengthening agricultural decisions in countries at risk of food insecurity: the GEOGLAM crop monitor for early warning. Remote Sens. Environ. 237, 111553.
- Boston, T., Van Dijk, A., Larraondo, P.R., Thackway, R., 2022. Comparing CNNs and random forests for landsat image segmentation trained on a large proxy land cover dataset. Remote Sens. 14 (14), 3396.
- Brandt, M., Tucker, C.J., Kariryaa, A., Rasmussen, K., Abel, C., Small, J., Chave, J., Rasmussen, L.V., Hiernaux, P., Diouf, A.A., Kergoat, L., Mertz, O., Igel, C., Gieseke, F., Schöning, J., Li, S., Melocik, K., Meyer, J., Sinno, S., Romero, E., Glennie, E., Montagu, A., Dendoncker, M., Fensholt, R., 2020. An unexpectedly large count of trees in the West African Sahara and Sahel. Nature 587, 78–82.
- Burke, M., Lobell, D.B., 2017. Satellite-based assessment of yield variation and its determinants in smallholder African systems. Proc. Natl. Acad. Sci. 114, 2189–2194.
- Burnett, M.W., White, T.D., McCauley, D.J., De Leo, G.A., Micheli, F., 2019. Quantifying coconut palm extent on Pacific islands using spectral and textural analysis of very high resolution imagery. Int. J. Remote Sens. 40, 7329–7355.
- Cheng, Y., Yu, L., Cracknell, A.P., Gong, P., 2016. Oil palm mapping using Landsat and PALSAR: a case study in Malaysia. Int. J. Remote Sens. 37, 5431–5442.

- Chivasa, W., Mutanga, O., Biradar, C., 2017. Application of remote sensing in estimating maize grain yield in heterogeneous African agricultural landscapes: a review. Int. J. Remote Sens. 38, 6816–6845.
- Cui, B., Huang, W., Ye, H., Chen, Q., 2022. The suitability of PlanetScope imagery for mapping rubber plantations. Remote Sens. 14, 1061.
- Descals, A., Szantoi, Z., Meijaard, E., Sutikno, H., Rindanata, G., Wich, S., 2019. Oil palm (Elaeis guineensis) mapping with details: smallholder versus industrial plantations and their extent in Riau, Sumatra. Remote Sens. 11, 2590.
- Dong, J., Xiao, X., Chen, B., Torbick, N., Jin, C., Zhang, G., Biradar, C., 2013. Mapping deciduous rubber plantations through integration of PALSAR and multi-temporal Landsat imagery. Remote Sens. Environ. 134, 392–402.
- Dong, J., Xiao, X., Sheldon, S., Biradar, C., Xie, G., 2012. Mapping tropical forests and rubber plantations in complex landscapes by integrating PALSAR and MODIS imagery. ISPRS J. Photogramm. Remote Sens. 74, 20–33.
- Duguma, L.A., Bah, A., Minang, P.A., Woldeyohanes, T., Jaiteh, M., Sanneh, E., Muthee, K., Badjie, M., 2021. In: Minang, P.A., Duguma, L.A., van Noordwijk, M. (Eds.), Cashew: An emerging tree commodity in African drylands for livelihoods improvement and ecosystem restoration. https://apps.worldagroforestry.org/downloads/Publications/PDFS/BC22001.pdf.
- Elshamli, A., Taylor, G.W., Berg, A., Areibi, S., 2017. Domain adaptation using representation learning for the classification of remote sensing images. IEEE JSel. Top. Appl. Earth Obs. Remote Sens. 10, 4198–4209.
- ESA Sentinel-2 User Handbook, 2015. Sentinel-2 User Handbook (accessed 05/25/2023). https://sentinel.esa.int/documents/247904/685211/Sentinel-2_User_Handbook.
- ESA, 2017. ESA CCI LC 2016 (accessed 05/20/2022). https://2016africalandcover20m. esrin.esa.int.
- ESA, 2021. ESA WorldCover 10 m 2020 (accessed 05/20/2022). https://esa-worldcover.
- Gal, Y., Ghahramani, Z., 2016. Dropout as a bayesian approximation: representing model uncertainty in deep learning. In: International conference on machine learning. PMLR, pp. 1050–1059.
- Gao, B.C., 1996. NDWI—A normalized difference water index for remote sensing of vegetation liquid water from space. Remote Sens. Environ. 58 (3), 257–266.
- Gascon, F., Bouzinac, C., Thépaut, O., Jung, M., Francesconi, B., Louis, J., Lonjou, V., Lafrance, B., Massera, S., Gaudel-Vacaresse, A., Languille, F., 2017. Copernicus sentinel-2A calibration and products validation status. Remote Sens. 9 (6), 584.
- Ghimire, B., Rogan, J., Miller, J., 2010. Contextual land-cover classification: incorporating spatial dependence in land-cover classification models using random forests and the getis statistic. Remote Sensing Letters 1 (1), 45–54.
- Ghamisi, P., Rasti, B., Yokoya, N., Wang, Q., Hofle, B., Bruzzone, L., Bovolo, F., Chi, M., Anders, K., Gloaguen, R., Atkinson, P.M., 2019. Multisource and multitemporal data fusion in remote sensing: a comprehensive review of the state of the art. IEEE Geosci. Remote Sens.Mag. 7 (1), 6–39.
- Ghosh, R., Ravirathinam, P., Jia, X., Lin, C., Jin, Z., Kumar, V., 2021. Attention-augmented spatio-temporal segmentation for land cover mapping. In: 2021 IEEE International Conference on Big Data (Big Data). IEEE, (1399–1408).
- Ghosh, R., Jia, X., Yin, L., Lin, C., Jin, Z., Kumar, V., 2022. Clustering augmented self-supervised learning: an application to land cover mapping. In: Proceedings of the 30th International Conference on Advances in Geographic Information Systems (1-10)
- Gomes, T., Freitas, E., Watanabe, P., Guerreiro, M., Sousa, A., Ferreira, A., 2018.

 Dehydrated cashew apple meal in the feeding of growing rabbits. Semina: Ciências Agrárias 39, 757.
- Gorelick, N., Hancher, M., Dixon, M., Ilyushchenko, S., Thau, D., Moore, R., 2017. Google Earth Engine: Planetary-scale geospatial analysis for everyone. Remote Sens. Environ 202. 18–27.
- Graves, A., Schmidhuber, J., 2005. Framewise phoneme classification with bidirectional LSTM and other neural network architectures. Neural Netw. 18, 602–610.
- Gutiérrez-Vélez, V.H., DeFries, R., 2013. Annual multi-resolution detection of land cover conversion to oil palm in the Peruvian Amazon. Remote Sens. Environ. 129, 154–167.
- Hall, D.K., Riggs, G.A., Salomonson, V.V., 1995. Development of methods for mapping global snow cover using moderate resolution imaging spectroradiometer data. Remote Sens. Environ. 54 (2), 127–140.
- Houborg, R., McCabe, M.F., 2018. A cubesat enabled patio-temporal enhancement method (CESTEM) utilizing planet, Landsat and MODIS data. Remote Sens. Environ. 209, 211–226.
- Hunt, D.A., Tabor, K., Hewson, J.H., Wood, M.A., Reymondin, L., Koenig, K., Schmitt-Harsh, M., Follett, F., 2020. Review of remote sensing methods to map coffee production systems. Remote Sens. 12, 2041.
- Hu, Q., Sulla-Menashe, D., Xu, B., Yin, H., Tang, H., Yang, P., Wu, W., 2019.
 A phenology-based spectral and temporal feature selection method for crop mapping from satellite time series. Int. J. Appl. Earth Obs. Geoinf. 80, 218–229.
- Jain, M., Mondal, P., DeFries, R.S., Small, C., Galford, G.L., 2013. Mapping cropping intensity of smallholder farms: a comparison of methods using multiple sensors. Remote Sens. Environ. 134, 210–223.
- Jain, M., Srivastava, A.K., Joon, R.K., McDonald, A., Royal, K., Lisaius, M.C., Lobell, D.B., 2016. Mapping smallholder wheat yields and sowing dates using micro-satellite data. Remote sens. 8 (10), 860.
- Ji, S., Zhang, C., Xu, A., Shi, Y., Duan, Y., 2018. 3D convolutional neural networks for crop classification with multi-temporal remote sensing images. Remote Sens. 10, 75.
- Jia, X., Khandelwal, A., Gerber, J., Carlson, K., West, P., Kumar, V., 2016. Learning large-scale plantation mapping from imperfect annotators. In: 2016 IEEE international conference on big data (big data). IEEE, pp. 1192–1201.

- Jia, X., Khandelwal, A., Carlson, K.M., Gerber, J.S., West, P.C., Samberg, L.H., Kumar, V., 2020. Automated plantation mapping in southeast Asia using modis data and imperfect visual annotations. Remote Sens. 12 (4), 636.
- Jia, X., Khandelwal, A., Nayak, G., Gerber, J., Carlson, K., West, P., Kumar, V., 2017. Incremental dual-memory lstm in land cover prediction. In: Proceedings of the 23rd ACM SIGKDD international conference on knowledge discovery and data mining (867-876).
- Jia, X., Li, S., Khandelwal, A., Nayak, G., Karpatne, A., Kumar, V., 2019. Spatial context-aware networks for mining temporal discriminative period in land cover detection. In: Proceedings of the 2019 SIAM International Conference on Data Mining (513-521): SIAM.
- Jin, Z., Azzari, G., You, C., Di Tommaso, S., Aston, S., Burke, M., Lobell, D.B., 2019. Smallholder maize area and yield mapping at national scales with Google Earth Engine. Remote Sens. Environ. 228, 115–128.
- Joyce, J.M., 2011. Kullback-leibler divergence. In: International Encyclopedia of Statistical Science. Springer, pp. 720–722.
- Kawakubo, F.S., Pérez Machado, R.P., 2016. Mapping coffee crops in southeastern Brazil using spectral mixture analysis and data mining classification. Int. J. Remote Sens. 37, 3414–3436.
- Kington IV, J.D., Jordahl IV, K.A., Kanwar IV, A.N., Kapadia IV, A., Schönert IV, M., Wurster IV, K., 2019. December. Spatially and Temporally Consistent Smallsat-Derived Basemaps for Analytic Applications. In: AGU Fall Meeting Abstracts, Vol. 2019. IN13B-0716.
- Kumar, S., Jayagopal, P., 2021. Delineation of field boundary from multispectral satellite images through U-Net segmentation and template matching. Ecol. Inf. 64, 101370.
- Lambert, M.-J., Traoré, P.C.S., Blaes, X., Baret, P., Defourny, P., 2018. Estimating smallholder crops production at village level from Sentinel-2 time series in Mali's cotton belt. Remote Sens. Environ. 216, 647–657.
- LeCun, Y., Bengio, Y., 1995. Convolutional networks for images, speech, and time series. In: The Handbook of Brain Theory and Neural Networks, 3361(10), p. 1995.
- Lin, C., Jin, Z., Mulla, D., Ghosh, R., Guan, K., Kumar, V., Cai, Y., 2021. Toward large-scale mapping of tree crops with high-resolution satellite imagery and deep learning algorithms: a case study of olive orchards in Morocco. Remote Sens. 13, 1740.
- Liu, S., Zhou, J., Qiu, Y., Chen, J., Zhu, X., Chen, H., 2022. The FIRST model: spatiotemporal fusion incorrporting spectral autocorrelation. Remote Sens. Environ. 279, 113111.
- Lowder, S.K., Skoet, J., Raney, T., 2016. The number, size, and distribution of farms, smallholder farms, and family farms worldwide. World Dev. 87, 16–29.
- Luong, M.-T., Pham, H., Manning, C.D., 2015. Effective approaches to attention-based neural machine translation. arXiv preprint arXiv:1508.04025.
- MacQueen, J., 1967. Classification and analysis of multivariate observations. In: 5th Berkeley Symp. Math. Statist. Probability (281-297).
- MAEP-Benin, 2017. Plan Stratégique de Développement du Secteur Agricole (PSDSA) 2025 et Plan National d'Investissements Agricoles et de Sécurité Alimentaire et Nutritionnelle PNIASAN (accessed 10/01/2022). https://ecowap.ecowas.int/media/ecowap/naip/files/BFNIN SIMfakD.pdf.
- MAEP-Benin, 2020. ETAT de MISE en ŒUVRE du Pag 2016–2021 accessed 10/01/2022. https://beninrevele.bj/doc/32/download.
- Maes, W.H., Steppe, K., 2019. Perspectives for remote sensing with unmanned aerial vehicles in precision agriculture. Trends Plant Sci. 24, 152–164.
- Martini, M., Mazzia, V., Khaliq, A., Chiaberge, M., 2021. Domain-adversarial training of self-attention-based networks for land cover classification using multi-temporal Sentinel-2 satellite imagery. Remote Sens. 13, 2564.
- Maskell, G., Chemura, A., Nguyen, H., Gornott, C., Mondal, P., 2021. Integration of sentinel optical and radar data for mapping smallholder coffee production systems in Vietnam. Remote Sens. Environ. 266, 112709.
- Masiza, W., Chirima, J.G., Hamandawana, H., Pillay, R., 2020. Enhanced mapping of a smallholder crop farming landscape through image fusion and model stacking. Int. J. Remote Sens. 41, 8739–8756.
- Mazzia, V., Khaliq, A., Chiaberge, M., 2019. Improvement in land cover and crop classification based on temporal features learning from Sentinel-2 data using recurrent-convolutional neural network (R-CNN). Appl. Sci. 10, 238.
- Meyfroidt, P., Vu, T.P., Hoang, V.A., 2013. Trajectories of deforestation, coffee expansion and displacement of shifting cultivation in the central highlands of Vietnam. Glob. Environ. Chang. 23 (5), 1187–1198.
- Mugabowindekwe, M., Brandt, M., Chave, J., Reiner, F., Skole, D., Kariryaa, A., Igel, C., Hiernaux, P., Ciais, P., Mertz, O., Tong, X., Li, S., Rwanyiziri, G., Dushimiyimana, T., Ndoli, A., Uwizeyimana, V., Lillesø, J.-P., Gieseke, F., Tucker, C., Saatchi, S., Fensholt, R., 2022. Nation-wide mapping of tree level carbon stocks in Rwanda. In: Research Square.
- NASA Landsat Next, 2022. Landsat next. https://landsat.gsfc.nasa.gov/satellites/landsat-next/accessed 05/25/2023.
- Nellis, M.D., Price, K.P., Rundquist, D., 2009. Remote sensing of cropland agriculture. In: The SAGE Handbook of Remote Sensing, 1, pp. 368–380.
- Nieke, J., Rast, M., 2018. Towards the copernicus hyperspectral imaging mission for the environment (CHIME). In: Igarss 2018–2018 ieee international geoscience and remote sensing symposium. IEEE, pp. 157–159.
- Olofsson, P., Foody, G.M., Stehman, S.V., Woodcock, C.E., 2013. Making better use of accuracy data in land change studies: estimating accuracy and area and quantifying uncertainty using stratified estimation. Remote Sens. Environ. 129, 122–131.
- Olofsson, P., Foody, G.M., Herold, M., Stehman, S.V., Woodcock, C.E., Wulder, M.A., 2014. Good practices for estimating area and assessing accuracy of land change. Remote Sens. Environ. 148, 42–57.
- Oreopoulos, L., Wilson, M.J., Várnai, T., 2011. Implementation on Landsat data of a simple cloud-mask algorithm developed for MODIS land bands. IEEE Geosci. Remote Sens. Lett. 8 (4), 597–601.

- Peña-Barragán, J.M., Ngugi, M.K., Plant, R.E., Six, J., 2011. Object-based crop identification using multiple vegetation indices, textural features and crop phenology. Remote Sens. Environ. 115 (6), 1301–1316.
- Pereira, S.C., Lopes, C., Pedro Pedroso, J., 2022. Mapping Cashew Orchards in Cantanhez National Park (Guinea-Bissau). Remote Sens. Appl.: Soc. Environ. 26, 100746.
- Planet, 2019. Planet basemaps product specification accessed 03/01/2023. https://asset s.planet.com/products/basemap/planet-basemaps-product-specifications.pdf.
- Planet, 2022a. PlanetScope constellation and sensor overview accessed 05/20/2022. htt ps://developers.planet.com/docs/data/planetscope/. accessed 05/20/2022.
- Planet, 2022b. Planet imagery product specification accessed 03/01/2023. https://assets.planet.com/docs/Planet_Combined_Imagery_Product_Specs_letter_screen.pdf.accessed 03/01/2023.
- Planet, 2022c. Scene level normalization and harmonization of planet dove imagery accessed 03/01/2023. https://assets.planet.com/docs/scene_level_normalization_of_planet_dove_imagery.pdf. accessed 03/01/2023.
- Planet, 2022d. SuperDove's 8 spectral bands accessed 05/20/2022. https://content.planet.com/c/65?x=XdDOks&lx=vlHTzf&mkt_tok=Otk3LUNISC0yNjUAAAGEChYFMnt1TyiacP7mjfeFdPERCL. 4teyoha44Y0aoY51LiSSymeU6vPJ4J2zZVRr3Q051pMo2dd9GRSUB68HjhjSDpQmduwQ3EggMLRkh2A.accessed 05/20/2022.
- Planet, 2022e. Next generation PlanetScope accessed 05/20/2022. https://www.planet.com/pulse/planet-launches-next-generation-planetscope-with-eight-spectral-bands-and-quality-improvements. accessed 05/20/2022.
- Pleiades, 2012. Pleiades imagery user guide accessed 03/01/2023. https://earth.esa.int/eogateway/documents/20142/37627/Pleiades-Imagery-User-Guide.pdf.
- PNIASAN-Benin, 2022. Benin/Regulatory framework for public and private investments: development of PNIASAN 3rd generation launched accessed 10/01/2022. https://www.jumelages-partenariats.com/en/actualites.php?n=16949.
- Preedy, V.R., Watson, R.R., 2020. Nuts and Seeds in Health and Disease Prevention.

 Academic Press.
- Putra, Y.C., Wijayanto, A.W., 2023. Automatic detection and counting of oil palm trees using remote sensing and object-based deep learning. Remote Sens.Appl.Soc. Environ. 29, 100914.
- Rafif, R., Kusuma, S.S., Saringatin, S., Nanda, G.I., Wicaksono, P., Arjasakusuma, S., 2021. Crop intensity mapping using dynamic time warping and machine learning from multi-temporal PlanetScope data. Land 10 (12), 1384.
- Rao, P., Zhou, W., Bhattarai, N., Srivastava, A.K., Singh, B., Poonia, S., Lobell, D.B., Jain, M., 2021. Using Sentinel-1, Sentinel-2, and planet imagery to map crop type of smallholder farms. Remote Sens. 13, 1870.
- Rege, A., Warnekar, S.B., Lee, J.S.H., 2022. Mapping cashew monocultures in the Western Ghats using optical and radar imagery in Google Earth Engine. Remote Sens.Appl.Soc.Environ. 28, 100861.
- Roy, D.P., Huang, H., Houborg, R., Martins, V.S., 2021. A global analysis of the temporal availability of PlanetScope high spatial resolution multi-spectral imagery. Remote Sens. Environ. 264, 112586.
- Ronneberger, O., Fischer, P., Brox, T., 2015. U-net: Convolutional networks for biomedical image segmentation. In: International Conference on Medical Image Computing and Computer-Assisted Intervention. Springer, (234–241).
- Rufin, P., Bey, A., Picoli, M., Meyfroidt, P., 2022. Large-area mapping of active cropland and short-term fallows in smallholder landscapes using PlanetScope data. Int. J. Appl. Earth Obs. Geoinf. 112, 102937.
- Samberg, L.H., Gerber, J.S., Ramankutty, N., Herrero, M., West, P.C., 2016. Subnational distribution of average farm size and smallholder contributions to global food production. Environ. Res. Lett. 11, 124010.
- Sanjeeva, S.K., Pinto, M.P., Narayanan, M.M., Kini, G.M., Nair, C.B., SubbaRao, P., Pullela, P.K., Ramamoorthy, S., Barrow, C.J., 2014. Distilled technical cashew nut shell liquid (DT-CNSL) as an effective biofuel and additive to stabilize triglyceride biofuels in diesel. Renew. Energy 71, 81–88.
- Schneibel, A., Stellmes, M., Röder, A., Frantz, D., Kowalski, B., Haß, E., Hill, J., 2017. Assessment of spatio-temporal changes of smallholder cultivation patterns in the angolan miombo belt using segmentation of landsat time series. Remote Sens. Environ. 195, 118–129.
- Shi, X., Chen, Z., Wang, H., Yeung, D.-Y., Wong, W.-K., Woo, W.-C., 2015. Convolutional LSTM network: A machine learning approach for precipitation nowcasting. Adv. Neural Inform. Process. Syst. 28.
- Singh, M., Evans, D., Chevance, J.-B., Tan, B.S., Wiggins, N., Kong, L., Sakhoeun, S., 2018. Evaluating the ability of community-protected forests in Cambodia to prevent deforestation and degradation using temporal remote sensing data. Ecol. Evol. 8, 10175–10191.
- Sishodia, R.P., Ray, R.L., Singh, S.K., 2020. Applications of remote sensing in precision agriculture: a review. Remote Sens. 12, 3136.

- Skole, D.L., Mbow, C., Mugabowindekwe, M., Brandt, M.S., Samek, J.H., 2021. Trees outside of forests as natural climate solutions. Nat. Clim. Chang. 11, 1013–1016.
- Somers, B., Asner, G.P., 2013. Multi-temporal hyperspectral mixture analysis and feature selection for invasive species mapping in rainforests. Remote Sens. Environ. 136, 14–27
- Stehman, S.V., 2014. Estimating area and map accuracy for stratified random sampling when the strata are different from the map classes. Int. J. Remote Sens. 35, 4923–4939.
- Tang, Y., Wang, Q., Tong, X., Atkinson, P.M., 2021. Integrating spatio-temporal-spectral information for downscaling Sentinel-3 OLCI images. ISPRS J. Photogramm. Remote Sens. 180, 130–150.
- Teluguntla, P., Thenkabail, P.S., Oliphant, A., Xiong, J., Gumma, M.K., Congalton, R.G., Yadav, K., Huete, A., 2018. A 30-m landsat-derived cropland extent product of Australia and China using random forest machine learning algorithm on Google Earth Engine cloud computing platform. ISPRS J. Photogramm. Remote Sens. 144, 325–340.
- Tridawati, A., Wikantika, K., Susantoro, T.M., Harto, A.B., Darmawan, S., Yayusman, L. F., Ghazali, M.F., 2020. Mapping the distribution of coffee plantations from multi-resolution, multi-temporal, and multi-sensor data using a random forest algorithm. Remote Sens. 12, 3933.
- Tuia, D., Persello, C., Bruzzone, L., 2016. Domain adaptation for the classification of remote sensing data: an overview of recent advances. IEEE Geosci. Remote Sens. Mag. 4, 41–57.
- UN, 2015. Sustainable Development Goals (accessed 05/20/2022). https://www.un.org/sustainabledevelopment.
- UNCTAD, 2021. Commodities at a Glance: special issue on cashew nuts accessed 05/20/2022. https://unctad.org/system/files/official-document/ditccom2020d1_en.pdf.
- Van der Maaten, L., Hinton, G., 2008. Visualizing data using t-SNE. J. Mach. Learn. Res.
- Vincenzi, S., Porrello, A., Buzzega, P., Cipriano, M., Fronte, P., Cuccu, R., Ippoliti, C., Conte, A., Calderara, S., 2021. The color out of space: learning self-supervised representations for earth observation imagery. In: 2020 25th International Conference on Pattern Recognition (ICPR). IEEE, (3034–3041).
- Waarts, Y., Janssen, V., Aryeetey, R., Onduru, D., Heriyanto, D., Aprillya, S., N'Guessan, A., Courbois, L., Bakker, D., Ingram, V., 2021. Multiple pathways towards achieving a living income for different types of smallholder tree-crop commodity farmers. Food Security 13, 1467–1496.
- Wei, S., Zhang, H., Wang, C., Wang, Y., Xu, L., 2019. Multi-temporal SAR data large-scale crop mapping based on U-net model. Remote Sens. 11, 68.
- Xie, J., Girshick, R., Farhadi, A., 2016. Unsupervised deep embedding for clustering analysis. In: International conference on machine learning. PMLR, pp. 478–487.
- Xu, J., Zhu, Y., Zhong, R., Lin, Z., Xu, J., Jiang, H., Huang, J., Li, H., Lin, T., 2020. DeepCropMapping: a multi-temporal deep learning approach with improved spatial generalizability for dynamic corn and soybean mapping. Remote Sens. Environ. 247, 111946.
- Xu, Y., Yu, L., Ciais, P., Li, W., Santoro, M., Yang, H., Gong, P., 2022. Recent expansion of oil palm plantations into carbon-rich forests. Nat. Sustainability 5, 574–577.
- Yamashita, R., Nishio, M., Do, R.K.G., Togashi, K., 2018. Convolutional neural networks: an overview and application in radiology. Insights into imaging 9, 611–629.
- Yan, L., Roy, D.P., Li, Z., Zhang, H.K., Huang, H., 2018. Sentinel-2A multi-temporal misregistration characterization and an orbit-based sub-pixel registration methodology. Remote Sens. Environ. 215, 495–506.
- Yin, L., You, N., Zhang, G., Huang, J., Dong, J., 2020. Optimizing feature selection of individual crop types for improved crop mapping. Remote Sens. 12, 162.
- You, N., Dong, J., 2020. Examining earliest identifiable timing of crops using all available sentinel 1/2 imagery and Google Earth Engine. ISPRS J. Photogramm. Remote Sens. 161, 109–123.
- Zhang, T., Wang, W., Wang, J., Cai, Y., Yang, Z., Li, J., 2022. Hyper-LGNet: coupling local and global features for hyperspectral image classification. Remote Sens. 14 (20), 5251.
- Zhou, J., Qiu, Y., Chen, J., Chen, X., 2021. A geometric misregistration resistant data fusion approach for adding red-edge (RE) and short-wave infrared (SWIR) bands to high spatial resolution imagery. Sci.Remote Sens. 4, 100033.
- Zeng, Y., Hao, D., Huete, A., Dechant, B., Berry, J., Chen, J.M., Joiner, J.,
 Frankenberg, C., Bond-Lamberty, B., Ryu, Y., Xiao, J., Asrar, G.R., Chen, M., 2022.
 Optical vegetation indices for monitoring terrestrial ecosystems globally. Nat. Rev. Earth Environ. 3, 477–493.
- Zou, K., Chen, X., Zhang, F., Zhou, H., Zhang, C., 2021. A field weed density evaluation method based on UAV imaging and modified U-net. Remote Sens. 13, 310.